Revised IMPROVE Algorithm for Estimating Light Extinction from Particle Speciation Data

I. Introduction

Light Extinction

Atmospheric light extinction is a fundamental metric used to characterize air pollution impacts on visibility. It is the fractional loss of intensity in a light beam per unit distance due to scattering and absorption by the gases and particles in the air. Light extinction (b_{ext}) can be expressed as the sum of light scattering by particles ($b_{s,p}$), scattering by gases ($b_{s,g}$), absorption by particles ($b_{a,p}$) and absorption by gases ($b_{a,g}$).*

Light extinction due to the gaseous components of the atmosphere are relatively well understood and well estimated for any atmospheric conditions. Absorption of visible light by gases in the atmosphere is primarily by NO_2, and can be directly and accurately estimated from NO_2 concentrations by multiplying by the absorption efficiency. Scattering by gases is described by the Rayleigh scattering theory (van de Hulst, 1981). Rayleigh scattering depends on the density of the atmosphere, with highest values at sea level (about $12Mm^{-1}$) and diminishing with elevation ($8Mm^{-1}$ at about 12,000'), and varies somewhat at any elevation due to atmospheric temperature and pressure variations. Rayleigh scattering can be accurately determined for any elevation and meteorological conditions.

Particle light extinction is more complex than that caused by gaseous components. Light-absorbing carbon (e.g. diesel exhaust soot and smoke) and some crustal minerals are the only commonly occurring airborne particle components that absorb light. All particles scatter light, and generally particle light scattering is the largest of the four light extinction components. If the index of refraction as a function of particle size is well characterized, Mie theory can be used to accurately calculate the light scattering and absorption by those particles. However, it is rare that these particle properties are known, so assumptions are used in place of missing information to develop a simplified calculation scheme that provides an estimate of the particle light extinction from the available data set.

Current Algorithm

IMPROVE particle monitoring provides 24-hour duration mass concentrations for PM_{10} and $PM_{2.5}$ as well as most of the $PM_{2.5}$ component concentrations on a one day in three schedule. These data are routinely available at each IMPROVE

* Light is a wavelength-dependent portion of the electro-magnetic spectrum. Traditionally for visibility-protection applications, the most sensitive portion of the spectrum for human vision (550nm) has been used to characterize light extinction and its components. For NO_2 light absorption, a photopic-weighted approach is used, as shown in section III.

monitoring site for use in estimating light extinction for the IMPROVE program. At 21 IMPROVE monitoring sites (Table A1 in appendix), hourly-averaged nephelometer and relative humidity data are also routinely available. Data from these sites have been key to evaluate the performance of the current IMPROVE algorithm, as well as for development and performance evaluation of proposed revised algorithms.

The current IMPROVE algorithm for estimating light extinction from IMPROVE particle monitoring data assumes that absorption by gases ($b_{a,g}$) is zero, that Rayleigh scattering ($b_{s,g}$) is 10Mm^{-1} for each monitoring site regardless of site elevation and meteorological condition, and that particle scattering and absorption ($b_{s,p}$ and $b_{a,p}$) can be estimated by multiplying the concentrations of each of six major components by typical component-specific light extinction efficiencies. The six major components are sulfate (assumed to be ammonium sulfate), nitrate (assumed to be ammonium nitrate), organic compounds (based on measured organic carbon mass), elemental or black carbon (directly measured), fine soil (crustal elements plus oxides) and coarse mass (the difference between PM_{10} and $PM_{2.5}$ mass concentrations). The component extinction efficiency values are constants, except for the sulfate and nitrate extinction efficiency terms that include a water growth factor that is a function of relative humidity (displayed as *f(RH)*) multiplied by a constant dry extinction efficiency. Monthly averaged water growth terms for each site were developed because most monitoring sites don't include on-site relative humidity monitoring. Expressed as an equation, the current algorithm for estimating light extinction from IMPROVE data takes the following form where the particle component concentrations are indicated in the brackets. The formulas for the composite components are available elsewhere (IMPROVE web site).

$$\begin{aligned} b_{ext} \approx\ & 3\times f(RH)\times[Sulfate] \\ & +3\times f(RH)\times[Nitrate] \\ & +4\times[Organic\ Mass] \\ & +10\times[Elemental\ Carbon] \\ & +1\times[Fine\ Soil] \\ & +0.6\times[Coarse\ Mass] \\ & +10 \end{aligned}$$

The units for light extinction and Rayleigh scattering are inverse megameters ($1/10^6$m usually written Mm^{-1}); component concentrations shown in brackets are in microgram per meter cubed (μg/m^3); dry efficiency terms are in units of meters squared per gram (m^2/g); and the water growth terms, f(RH), are unitless.

Among the implicit assumptions for this formulation of the algorithm are that

- the six particle component terms plus a constant Rayleigh scattering term are sufficient for a good estimate of light extinction;

- constant dry extinction efficiency terms rounded to one significant digit for each of the six particle components (i.e. for both sulfate and nitrate the value is 3) works adequately for all locations and times; and
- light extinction contributed by the individual particle components can be adequately estimated as separate terms as they would if they were in completely separate particles (externally mixed), though they often are known to be internally mixed in particles.

A relatively simple algorithm for estimating light extinction using only the available monitoring data requires assumptions such as these.

Estimates of particle scattering by this algorithm (i.e. excluding the light absorbing carbon and Rayleigh terms) have been compared to directly-measured particle scattering data at the 21 monitoring sites that have hourly-averaged nephelometer and relative humidity data. As shown in Figure 1 below, the algorithm performs reasonably well over a broad range of particle light scattering values and monitoring locations. The algorithm tends to under-estimate the highest extinction values and over-estimate the lowest extinction values. Since it first use (IMPROVE Report, 1993), the current algorithm has been a useful tool that contributed significantly to a better understanding of haze levels and the relative magnitude of haze contribution by the various particle components.

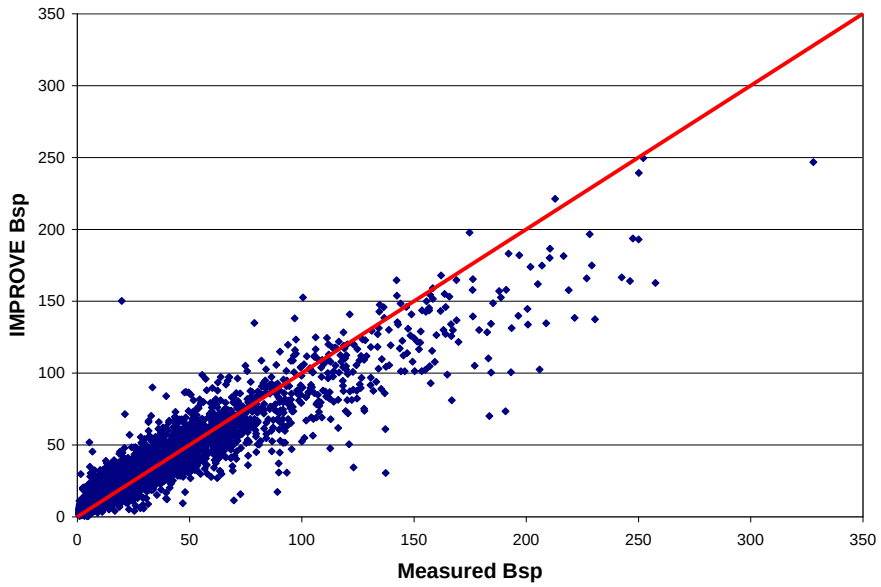

Figure 1. A scatter plot of the current IMPROVE algorithm estimated particle light scattering versus measured particle light scattering.

Review and Revision

The IMPROVE algorithm for estimating light extinction was adopted by the EPA as basis for the regional haze metric used to track progress in reducing haze levels for visibility-protected areas under the 1999 Regional Haze Rule (RHR).

As a result the IMPROVE algorithm has been scrutinized carefully to assess deficiencies that could bias the implementation of the RHR.

The RHR uses the IMPROVE algorithm to estimate light extinction, which is then converted to the deciview haze index (i.e. a logarithmic transformation of b_{ext}). The RHR then calls for the determination of the mean of the annual 20% best and 20% worst haze days for each of the IMPROVE monitoring sites that represent the visibility-protected areas. States are asked to manage emissions so that over a 60-year period the worst haze days will improve to natural conditions without degrading visibility conditions for the best haze days. For consistency, the same approach (i.e. IMPROVE algorithm and conversion to the deciview haze index) is also used to estimate natural haze levels for each representative monitoring site using estimates of the natural concentration levels for the major particle components. For each location, the linear rate of reduction of the deciview values for the worst haze days during the baseline period (2000 to 2004) that is needed to reach the estimated worst haze days under natural conditions by 2064 must be determined. This linear rate is used as a guide to pace the desired rate of haze reduction and to determine interim visibility goals that are compared to the monitoring data trends of the best and worst haze days.

The RHR emphasizes the extremes of light extinction through its requirement to estimate best and worst haze days for the baseline period and for estimates of natural worst haze conditions. Also, the use of the deciview index means that additive biases in the light extinction estimates (e.g. the use of a standard Rayleigh scattering term for all sites regardless of elevation) will affect the calculation of a linear glide slope, which is used to set the pace of emission reductions. Use of the IMPROVE algorithm for the RHR elicited concerns about possible biases in the apportionment among the various major particle components. Such issues have been the subject of a number of critical reviews of the use of the IMPROVE algorithm in the RHR (Lowenthal and Kumar, 2003; Ryan et al., 2005).

In light of the concerns raised by its use in the RHR, the IMPROVE Steering Committee initiated an internal review including recommendations for revisions of the IMPROVE algorithm for estimating light extinction. The review team (composed of National Park Service and Cooperative Institute for Research in the Atmosphere scientists) reviewed pertinent literature and employed both Mie theory modeling and statistical assessment methods to identify deficiencies in the current algorithm and evaluate possible refinements. The goal was to develop a revised algorithm that reduces biases in light extinction estimates, and is as consistent as possible with the current scientific literature while constrained by the need to use only those data that are routinely available from the IMPROVE particle monitoring network. A preliminary report by this team was presented in June, 2005 at a national Regional Planning Organization workshop in Denver Colorado hosted by the Western Regional Air Partnership (WRAP) and broadly participated in by those with an interest in the regional haze rule. The preliminary

results were also summarized in presentations at the July 2005 IMPROVE Steering Committee meeting in Acadia Maine. The full report of this review is available elsewhere (Hand and Malm, 2005).

Purpose and Organization

This document is a summary report by a subcommittee established by the IMPROVE Steering Committee at their July 2005 meeting to recommend a refined algorithm that would replace or be made available as an alternative to the current approach. The subcommittee included those who worked on the internal review as well as scientists who have been critical of the original IMPROVE algorithm.† The primary purpose of this document is to describe the subcommittee's recommended revised algorithm, characterize its performance, and summarize the rationale for each of the changes from the currently used algorithm. This document is the principal means to communicate the recommendations to the IMPROVE Steering Committee prior to their deliberation and vote on the adoption of a new algorithm. Others with an interest in this topic, including those who have responsibilities or interests associated with the RHR may also find it to be useful in understanding the technical issues and how the recommended algorithm addresses them.

Section II of the report describes the recommended revised algorithm for estimating light extinction using IMPROVE particle data and shows its performance compared to that of the currently used approach. Section III provides the technical justification of each of the revised terms in the recommended algorithm.

REFERENCES

Hand, J.L. and W.C. Malm, 2005: Review of the IMPROVE Equation for Estimating Ambient Light Extinction Coefficients, on the IMPROVE web site at http://vista.cira.colostate.edu/improve/Publications/GrayLit/gray_literature.htm

Lowenthal, D.H. and Kumar, N., 2003: $PM_{2.5}$ mass and light extinction reconstruction in IMPROVE. *J. Air & Waste Manage. Assoc.* ***53,*** 1109-1120.

Ryan, P.A., Lowenthal, D., and Kumar, N., 2005: Improved light extinction reconstruction in Interagency Monitoring of Protected Visual Environments. *J. Air & Waste Manage. Assoc.* **55**, 1751-1759.

van de Hulst, H. C., *Light scattering by small particles,* New York: Dover, 1981

† Subcommittee members concurring in these recommendations are William Malm and Bret Schichtel, NPS; Marc Pitchford, NOAA; Naresh Kumar, EPRI; Douglas Lowenthal, DRI; and Jenny Hand, CIRA

II. Overview of the Revised Algorithm

The recommended revised algorithm is shown in the equation below with revised terms in bold font. The total sulfate, nitrate and organic carbon compound concentrations are each split into two fractions, representing small and large size distributions of those components. Though not explicitly shown in the equation, the organic mass concentration used in this new algorithm is 1.8 times the organic carbon mass concentration, changed from 1.4 times carbon mass concentration as used for input for the current IMPROVE algorithm. New terms have been added for sea salt (important for coastal locations) and for absorption by NO_2 (only used where NO_2 data are available). Site-specific Rayleigh scattering is calculated for the elevation and annual average temperature of each of the IMPROVE monitoring sites as shown in the Table A at the end of the document.

$$
\begin{aligned}
b_{ext} \approx\ & \mathbf{2.2 \times f_S(RH) \times [Small\ Sulfate]} + \mathbf{4.8 \times f_L(RH) \times [Large\ Sulfate]} \\
& + \mathbf{2.4 \times f_S(RH) \times [Small\ Nitrate]} + \mathbf{5.1 \times f_L(RH) \times [Large\ Nitrate]} \\
& + \mathbf{2.8 \times [Small\ Organic\ Mass]} + \mathbf{6.1 \times [Large\ Organic\ Mass]} \\
& + 10 \times [Elemental\ Carbon] \\
& + 1 \times [Fine\ Soil] \\
& + \mathbf{1.7 \times f_{SS}(RH) \times [Sea\ Salt]} \\
& + 0.6 \times [Coarse\ Mass] \\
& + \mathbf{Rayleigh\ Scattering\ (Site\ Specific)} \\
& + \mathbf{0.33 \times [NO_2\ (ppb)]}
\end{aligned}
$$

The apportionment of the total concentration of sulfate compounds into the concentrations of the small and large size fractions is accomplished using the following equations.

$$[Large\ Sulfate] = \frac{[Total\ Sulfate]}{20 \mu g/m^3} \times [Total\ Sulfate], \quad for\ [Total\ Sulfate] < 20 \mu g/m^3$$

$$[Large\ Sultate] = [Total\ Sulfate] \quad for\ [Total\ Sulfate] \geq 20 \mu g/m^3$$

$$[Small\ Sulfate] = [Total\ Sulfate] - [Large\ Sulfate]$$

The same equations are used to apportion total nitrate and total organic mass concentrations into the small and large size fractions.

Sea salt is calculated as 1.8 x [*Chloride*], or 1.8 x [*Chlorine*] if the chloride measurement is below detection limits, missing or invalid. The algorithm uses three water growth adjustment term as shown in the Figure 2 and Table 1. They

are for use with the small size distribution and the large size distribution sulfate and nitrate compounds and for sea salt ($f_S(RH)$, $f_L(RH)$ and $f_{SS}(RH)$ respectively).

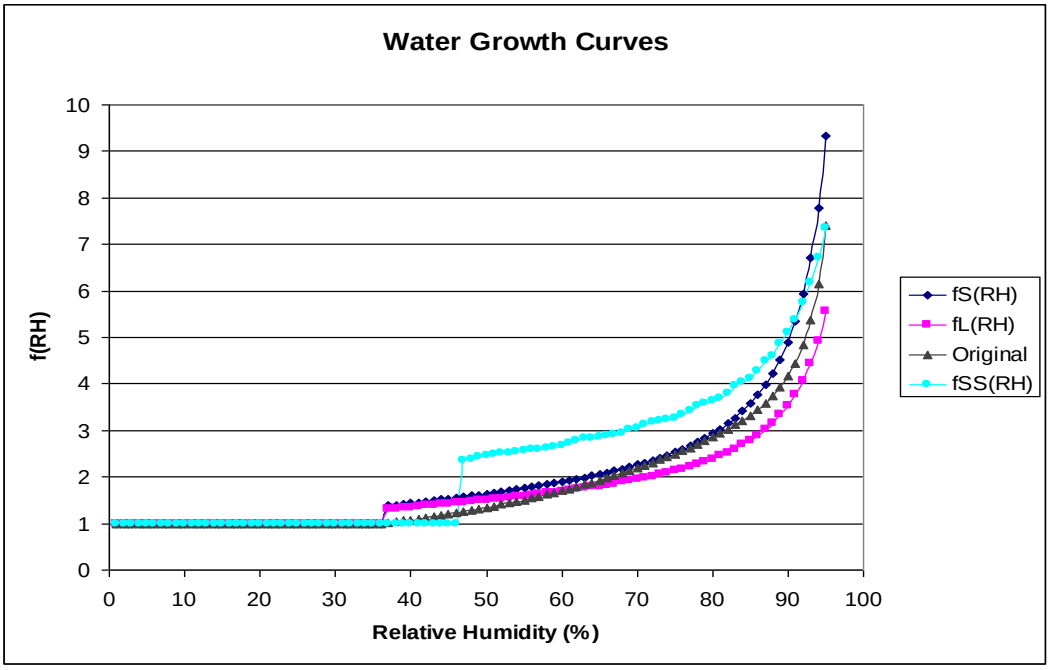

Figure 2. Water growth curves for small and large size distribution sulfate and nitrate, sea salt and the original IMPROVE algorithm sulfate and nitrate.

Table 1. f(RH) for small and large size distribution sulfate and nitrate, an sea salt.

RH (%)	$f_S(RH)$	$f_L(RH)$	$f_{SS}(RH)$	RH (%)	$f_S(RH)$	$f_L(RH)$	$f_{SS}(RH)$	RH (%)	$f_S(RH)$	$f_L(RH)$	$f_{SS}(RH)$
0 to 36	1.00	1.00	1.00	**56**	1.78	1.61	2.58	**76**	2.60	2.18	3.35
37	1.38	1.31	1.00	**57**	1.81	1.63	2.59	**77**	2.67	2.22	3.42
38	1.40	1.32	1.00	**58**	1.83	1.65	2.62	**78**	2.75	2.27	3.52
39	1.42	1.34	1.00	**59**	1.86	1.67	2.66	**79**	2.84	2.33	3.57
40	1.44	1.35	1.00	**60**	1.89	1.69	2.69	**80**	2.93	2.39	3.63
41	1.46	1.36	1.00	**61**	1.92	1.71	2.73	**81**	3.03	2.45	3.69
42	1.48	1.38	1.00	**62**	1.95	1.73	2.78	**82**	3.15	2.52	3.81
43	1.49	1.39	1.00	**63**	1.99	1.75	2.83	**83**	3.27	2.60	3.95
44	1.51	1.41	1.00	**64**	2.02	1.78	2.83	**84**	3.42	2.69	4.04
45	1.53	1.42	1.00	**65**	2.06	1.80	2.86	**85**	3.58	2.79	4.11
46	1.55	1.44	1.00	**66**	2.09	1.83	2.89	**86**	3.76	2.90	4.28
47	1.57	1.45	2.36	**67**	2.13	1.86	2.91	**87**	3.98	3.02	4.49
48	1.59	1.47	2.38	**68**	2.17	1.89	2.95	**88**	4.23	3.16	4.61
49	1.62	1.49	2.42	**69**	2.22	1.92	3.01	**89**	4.53	3.33	4.86
50	1.64	1.50	2.45	**70**	2.26	1.95	3.05	**90**	4.90	3.53	5.12
51	1.66	1.52	2.48	**71**	2.31	1.98	3.13	**91**	5.35	3.77	5.38
52	1.68	1.54	2.50	**72**	2.36	2.01	3.17	**92**	5.93	4.06	5.75
53	1.71	1.55	2.51	**73**	2.41	2.05	3.21	**93**	6.71	4.43	6.17
54	1.73	1.57	2.53	**74**	2.47	2.09	3.25	**94**	7.78	4.92	6.72
55	1.76	1.59	2.56	**75**	2.54	2.13	3.27	**95**	9.34	5.57	7.35

Algorithm Performance Evaluation

Performance of the current and proposed new algorithm for estimating extinction can be assessed in a number of ways each of which serves to answer different questions. Reduction of the biases in light scattering estimates at the extremes (i.e. underestimation of the high values and over estimation of the low values) when compared to nephelometer measurements was one of the most compelling reasons for development of a new algorithm, so comparisons of bias for the current and proposed new algorithm are one way to evaluate performance.

The fractional bias for each sample period was calculated as the difference in light scattering (i.e. estimated b_{sp} minus the measured b_{sp}) divided by the measured light scattering. These biases were then averaged in each quintile to indicate the bias in those five subsets of the data from the lowest to the highest light scattering values. Two different approaches to this grouping by quintiles were performed, referred to as criteria 1 and 2.

Criterion 1 used the measured light scattering to determine which sample periods were in each quintile. Since we think of the nephelometer as the better measure of light scattering, bias by this criterion better addresses the question of algorithm performance with regards to the haze conditions. Criterion 2 uses the algorithm-estimated light extinction to determine which sample periods were in each quintile. The Regional Haze Rule index is based on the highest and lowest haze levels as determined by the algorithm, so criterion 2 better addresses the haze rule application of the algorithm. Tables 2 through 5 show the bias results by both criteria for the current and new algorithm for sites averaged by RPO.

Table 2. Averaged fractional bias by RPO for the current IMPROVE algorithm with quintiles based on measured light scattering (criterion 1). Bold font highlights the bias values that are lower than corresponding values in Table 3.

RPO	Quintile 1	Quintile 2	Quintile 3	Quintile 4	Quintile 5	Average
CEN	0.67	0.18	0.10	**0.02**	-0.11	0.17
MANE	0.93	0.27	0.19	0.10	**0.01**	0.28
VISTAS	0.59	0.21	0.11	**0.02**	-0.13	0.16
WRAP	1.07	0.37	0.18	0.07	**-0.08**	0.32

Table 3. Averaged fractional bias by RPO for the current new proposed algorithm with quintiles based on measured light scattering (criterion 1). Bold font highlights the bias values that are lower than corresponding values in Table 2.

RPO	Quintile 1	Quintile 2	Quintile 3	Quintile 4	Quintile 5	Average
CEN	**0.51**	**0.08**	**0.02**	-0.03	**-0.08**	**0.10**
MANE	**0.74**	**0.14**	**0.06**	**0.01**	-0.02	**0.17**
VISTAS	**0.50**	**0.16**	0.11	0.06	**-0.01**	0.16
WRAP	**0.84**	**0.25**	**0.08**	**0.01**	-0.10	**0.21**

Table 4. Averaged fractional bias by RPO for the current IMPROVE algorithm with quintiles based on estimated light scattering (criterion 2). Bold font highlights the bias values that are lower than corresponding values in Table 5.

RPO	Quintile 1	Quintile 2	Quintile 3	Quintile 4	Quintile 5	Average
CEN	0.42	0.19	0.18	0.09	**-0.01**	0.17
MANE	0.35	0.27	0.30	0.33	**0.15**	0.28
VISTAS	0.38	0.19	0.14	**0.08**	**0.01**	0.16
WRAP	0.58	0.37	0.26	0.25	**0.15**	0.32

Table 5. Averaged fractional bias by RPO for the current new proposed algorithm with quintiles based on estimated light scattering (criterion 2). Bold font highlights the bias values that are lower than corresponding values in Table 4.

RPO	Quintile 1	Quintile 2	Quintile 3	Quintile 4	Quintile 5	Average
CEN	**0.23**	**0.11**	**0.08**	**0.06**	0.02	**0.10**
MANE	**0.15**	**0.14**	**0.15**	**0.19**	0.21	**0.17**
VISTAS	**0.25**	**0.14**	**0.08**	0.13	0.21	0.16
WRAP	**0.37**	**0.19**	**0.19**	**0.16**	0.17	**0.21**

These tables show that the new algorithm has lower fractional bias than the current IMPROVE algorithm in all but the haziest conditions (i.e. quintile 5) regardless of the criterion used to sort the data into quintiles. By criterion 1, the two algorithms perform about the same for haziest days except for the sites in the southeastern U.S. (i.e. the VISTA RPO), where the new algorithm has much lower bias (1% compared to 13%). Using criterion 2, the current algorithm has consistently lower bias compared with the new algorithm for the haziest days (i.e. quintile 5) for each of the RPOs. This seeming paradox is the result of the somewhat greater imprecision of the new algorithm compared to the current algorithm, which results in somewhat larger errors in selecting worst haze sample periods for the new algorithm compared with the current algorithm.

Scatter plots (Figures 1 and 3) of light scattering estimates from the current and new proposed algorithms versus nephelometer data for all available data at 21 monitoring sites are one way to view the overall performance differences between the two. These figures show that the bias at the extremes is reduced using the new algorithm compared to the original IMPROVE algorithm (i.e. the points tend to be better centered on the one-to-one line). They also show that the somewhat reduced precision of the new algorithm compared to the original IMPROVE algorithm (i.e. points are more broadly scattered).

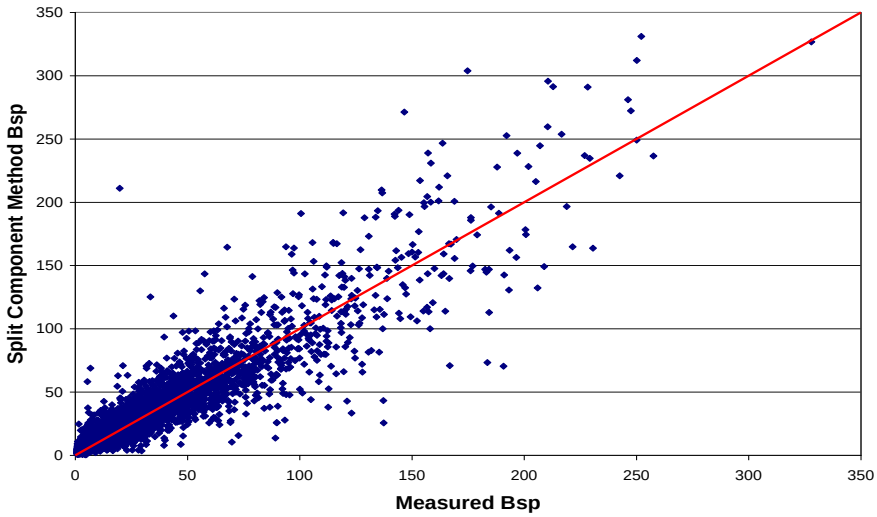

Figure 3. Scatter plot of the recommended revised algorithm estimates of light scattering versus measured light scattering.

Similar pairs of scatter plots were prepared for each individual monitoring site (available in the appendix). Figures 4 and 5 are example plots for Shenandoah and Grand Canyon National Parks. The logarithmic scales on these plots exaggerate the scatter for low values compared to high values. The individual-site scatter plots have the 80th percentile values indicated on the graphs for the predicted and measured values by horizontal and vertical lines respectively. Points that are to the right of the vertical line have nephelometer values that are among the 20% worst light scattering for that monitoring sites. Points that are above the horizontal line have algorithm determined values that are among the 20% worst estimated light scattering for that monitoring site.

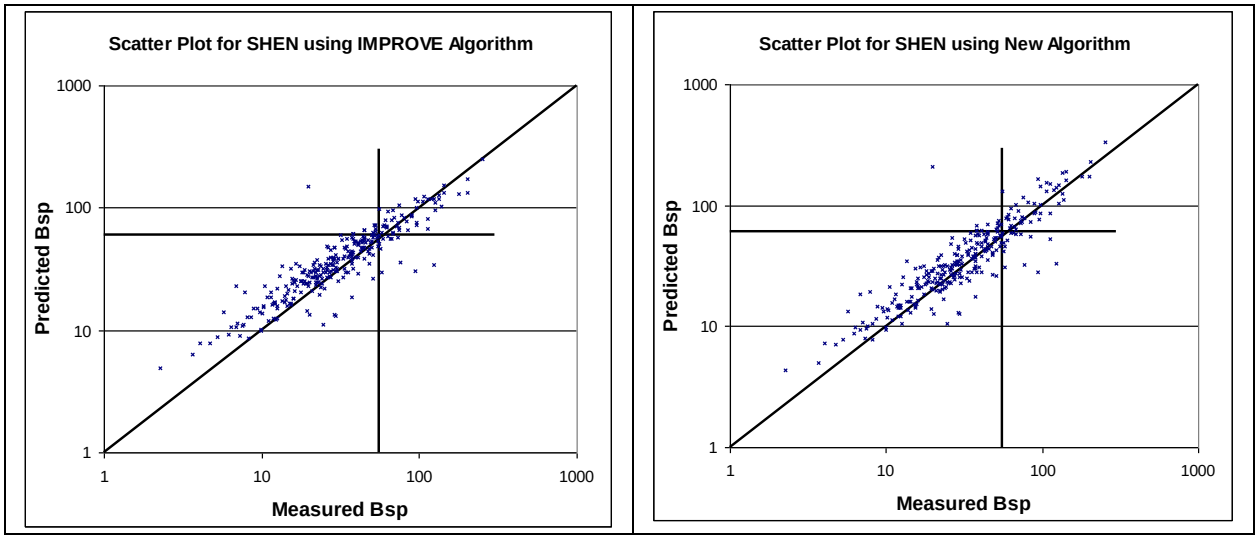

Figure 4. Scatter plots of the current IMPROVE and new recommended algorithm estimates of light scattering versus measured light scattering for Shenandoah National Park. Horizontal and vertical lines are at the 80th percentile for estimated and measured light scattering.

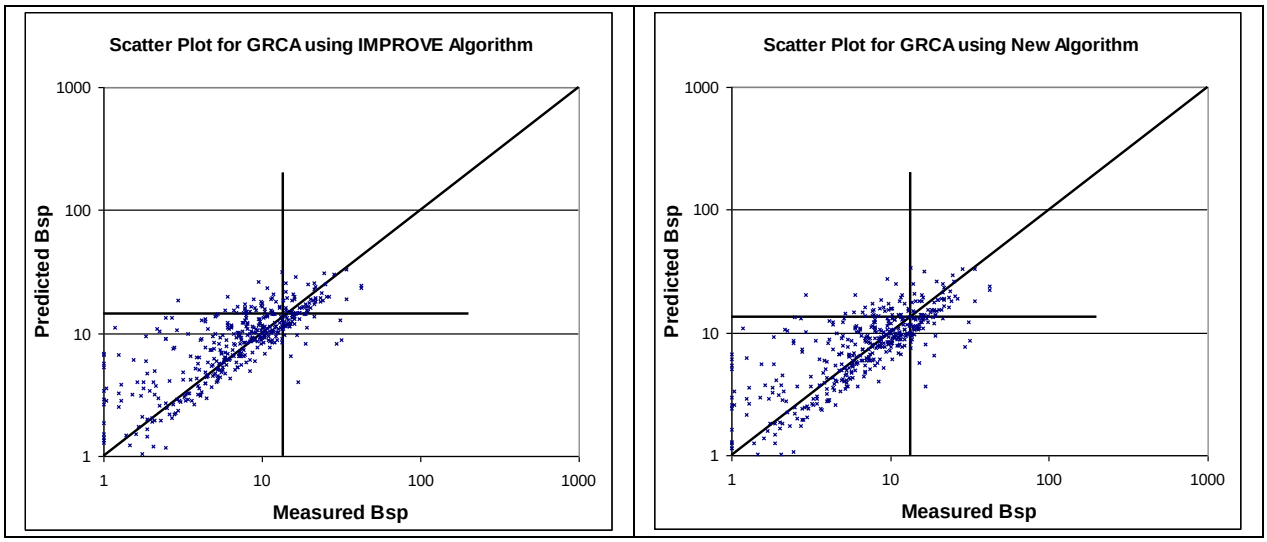

Figure 5. Scatter plots of the current IMPROVE and new recommended algorithm estimates of light scattering versus measured light scattering for Grand Canyon National Park. Horizontal and vertical lines are at the 80th percentile for estimated and measured light scattering.

The proposed new algorithm performs noticeably better with respect to having data points more centered on the one-to-one line at the high and low haze level extremes than the current IMPROVE algorithm for Shenandoah National Park, which is typical for the high haze level locations in the southeast U.S. A large number of the measured worst haze sample periods are correctly identified by both algorithms (these are the points above and to the right of the two 80th percentile lines). The differences between the two algorithms for Grand Canyon National Park and most of the other less hazy locations are not apparent in these scatter plots.

The final approach for evaluating the relative performance of the two algorithms is to compare the average composition of the best haze days and the worst haze days as selected using each algorithm and using the measured light scattering. Table 6 and 7 contain the average composition by RPO for days selected as best and worst by these three methods. Similar results for each of the 21 nephelometer monitoring locations are shown in tables in the appendix.

Table 6. Mean light scattering and percent $PM_{2.5}$ composition for the five major components for 20% best days as determined by measurement, the current IMPROVE algorithm and the proposed new algorithm.

RPO		Mean Bsp (Mm-1)	Percent Ammonium Sulfate	Percent Ammonium Nitrate	Percent OCM	Percent Soil	Percent Coarse	Percent EC
	Measured	6.8	19	2	15	8	54	2
CENRAP	IMPROVE	9.1	20	2	15	7	53	2
	NEW	8.1	21	3	16	7	51	2

	Measured	6.1	22	3	22	4	47	3
MANEVU	IMPROVE	8.4	21	3	22	4	47	3
	NEW	7.4	22	4	22	4	45	3
	Measured	13.8	25	7	21	4	40	3
VISTAS	IMPROVE	18.4	25	7	21	4	40	3
	NEW	17.0	25	8	21	4	39	3
	Measured	3.4	13	3	18	8	55	3
WRAP	IMPROVE	5.2	14	3	19	8	53	3
	NEW	4.5	15	3	19	8	52	3

Table 7. Mean light scattering and percent $PM_{2.5}$ composition for the five major components for 20% worst days as determined by measurement, the current IMPROVE algorithm and the proposed new algorithm.

RPO		Mean Bsp (Mm-1)	Percent Ammonium Sulfate	Percent Ammonium Nitrate	Percent OCM	Percent Soil	Percent Coarse	Percent EC
	Measured	76	34	6	19	5	34	2
CENRAP	IMPROVE	67	34	6	19	5	33	2
	NEW	72	34	6	19	6	34	2
	Measured	61	36	6	23	3	30	3
MANEVU	IMPROVE	61	36	6	22	3	30	3
	NEW	63	35	6	23	3	31	3
	Measured	120	46	5	21	3	22	2
VISTAS	IMPROVE	106	47	4	21	3	23	2
	NEW	127	47	3	22	3	22	2
	Measured	36	15	6	27	7	42	3
WRAP	IMPROVE	33	14	6	27	6	44	3
	NEW	33	13	6	27	6	44	3

These tables demonstrate that the composition associated with the best and worst haze days are not very sensitive to the method of identifying the sample periods that fit in best and worst categories. Some of the individual sites (e.g. Grand Canyon) have somewhat larger variations in the composition between measurement-selected days compared to algorithm-selected days, though there's little difference between the average composition comparing the two algorithms on the best and worst days. The contributions to light extinction by the various components were not explicitly calculated, but are inherently somewhat different because of the explicit differences in the two algorithms.

In summary, the proposed new algorithm for estimating haze reduces the biases compared to measurements at the high and low extremes. This is most apparent for the hazier eastern sites. The composition of days selected as best and worst by the current and the new algorithm are very similar, and similar to days selected by measurements. Most of the reduction of bias associated with the new algorithm is attributed to the use of the split component extinction efficiency method for sulfate, nitrate and organic components that permitted variable extinction efficiency depending on the component mass concentration. Though

not subject to explicit performance testing, the proposed new algorithm also contains specific changes from the current algorithm that reflect a better understanding of the atmosphere as reflected in the more recent scientific literature (e.g. change to 1.8 from 1.4 for organic compound mass to carbon mass ratio) and a more complete accounting for contributors to haze (e.g. sea salt and NO_2 terms), and use of site specific Rayleigh scattering terms to reduce elevation-related bias.

III. Technical Justification for Revisions

Five major revisions to the IMPROVE algorithm for estimating light extinction from IMPROVE particle speciation data are incorporated into the recommended approach. They include

- addition of a **sea salt** term which is a particular concern for coastal monitoring locations where the sum of the major components of light extinction and mass have been deficient;
- change the assumed **organic mass to organic carbon ratio** from 1.4 to 1.8 to reflect more recent peer-reviewed literature on the subject;
- use of **site-specific Rayleigh scattering** based on the elevation and annual average temperature of the monitoring sites;
- development and use of a **split component extinction efficiency model for sulfate, nitrate and organic carbon components** including new water growth terms for sulfate and nitrate to better estimate light extinction at the high and low extremes of the range; and
- addition of a **NO_2 light absorption term** that would only be used at sites with available NO_2 concentration data.

A summary of the technical rationale for making each of these changes is described in separate sections below.

<u>Sea Salt</u>

The current IMPROVE protocol for estimating light extinction does not include light scattering (b_{sp}) by sea salt aerosols. Lowenthal and Kumar (2003) demonstrated that inclusion of elements from sea salt (e.g., Na, Cl) increased the accuracy of mass reconstruction at coastal IMPROVE sites. Contributions of sea salt particles to light extinction at some coastal IMPROVE sites may be significant, especially since b_{sp} by sea salt particles should be significantly enhanced by hygroscopic growth in humid environments. Lowenthal and Kumar (2005) found that fine sea salt aerosols accounted for 43% of estimated b_{sp} at the U.S. Virgin Islands IMPROVE site.

To include sea salt in the IMPROVE light extinction equation, it is necessary to: 1) estimate the sea salt mass concentration; 2) specify a dry sea salt scattering efficiency; and 3) specify an f(RH) curve for sea salt representing the

enhancement of sea salt scattering by hygroscopic growth as a function of relative humidity (RH).

Sea Salt Mass Concentration

Estimating sea salt mass requires a sea salt marker species measured in IMPROVE aerosol samples. The most obvious such markers are sodium (Na) and chlorine (Cl), since NaCl is the main component in sea water and sea salt. Based on the composition of sea water, pure sea salt mass is Na multiplied by 3.1 or Cl multiplied by 1.8 (Pytkowicz and Kester, 1971). However, Na is poorly quantified by x-ray fluorescence (XRF) and Cl can be depleted in ambient aerosol samples by acid-base reactions between sea salt particles and sulfuric and nitric acids (McInnes et al., 1994). Without accurate measurement of both Na (or other conservative tracers) and Cl, it is not possible to estimate how much Cl has been replaced by nitrate and/or sulfate in ambient samples. Further, without chemical speciation of the PM_{10} sample (Module D of the IMPROVE sampler), it is not possible to estimate coarse sea salt scattering.

Given these limitations, it is recommended that the $PM_{2.5}$ sea salt concentration be estimated as the concentration of chloride ion (Cl^-) measured by ion chromatography multiplied by 1.8. If the chloride measurement is below the detection limit, missing or invalid then the $PM_{2.5}$ sea salt concentration should be estimated as the concentration of chlorine (Cl) measured by XRF multiplied by 1.8.

Although the XRF measurement can detect chlorine (Cl) at lower concentrations, the A-module sample for XRF is more exposed to reactive losses because acidic gases are not removed from the air-stream and any HCl they release from the sample is not retained by the Teflon filter. Unless speciated data become available for PM_{10}, coarse sea salt mass and light scattering will not be considered. To the degree that chloride has been replaced by sulfate or nitrate in ambient particles, this approach will underestimate the mass and scattering contributed by the substituted sea salt that results (e.g. $NaNO_3$, $NaHSO_4$, or Na_2SO_4). This mass is partially accounted for by ammonium sulfate and ammonium nitrate in the IMPROVE equation. However, the substituted Na salt mass is under-estimated because ammonium is lighter than sodium. The scattering is also under-estimate because the sodium salts absorb more water than does ammonium sulfate above 60% RH. Given the limitations of the available data, 1.8 times chloride provides a reasonable lower-limit to the fine sea salt mass.

Dry Scattering Efficiency

In order to estimate the dry scattering efficiency and f(RH) for sea salt aerosols, their dry mass size distribution must be known. While this has not been measured at most IMPROVE sites, extensive sea salt size distribution measurements have been made in the remote marine environment during cruised-based experiments (Quinn et al., 1995, 1996, 1998). Based on these

studies, a dry log-normal mass size distribution with a geometric mean diameter (D_g) of 2.5 µm and geometric standard deviation (σ_g) of 2 is recommended. A dry scattering efficiency for $PM_{2.5}$ sea salt of 1.7 m^2/g was calculated using Mie theory based on this size distribution assuming a sea salt refractive index of [1.55+ i0] and a density of 1.9 g cm^{-3} recommended by Quinn et al. (1995).

Sea Salt f(RH)

Tang et al. (1997) determined hygroscopic growth curves for aerosols generated from Long Island, NY and Atlantic Ocean seawater. The water absorption curves for sea salt were nearly identical to that of NaCl. The NaCl growth factors derived from the AIM3 thermodynamic equilibrium model (Clegg et al., 1998) are shown in Table 8 as a function of relative humidity (RH). Below the crystallization point (RH = 47%), the growth factor set to one. Values are presented to RH = 95% , to which higher RH are "rolled back" under the Regional Haze Rule protocol (USEPA, 2001). Dry (RH=0%) light scattering ($b_{sp(Dry)}$) was calculated using Mie theory for sea salt at unit $PM_{2.5}$ mass concentration with the dry mass size distribution, refractive index, and density described above. Light scattering at RH = 46-95% at unit RH intervals ($b_{sp(RH)}$) was calculated by applying the NaCl growth curve (Table 8) to the dry mass size distribution using Mie theory, accounting for the change in particle volume and refractive index from the addition of water. The f(RH) values, defined as $b_{sp(RH)}/b_{sp(Dry)}$, are listed in Table 8. The f(RH) values in Table 8 will be converted to monthly, site-specific "climatological" values, as was done for ammonium sulfate/ammonium nitrate. Light scattering by sea salt (SS) aerosols is estimated as:

$$b_{sp(SS)} = 1.7\, f_{SS}(RH)\, [1.8 * Cl].$$

Table 8. Sea Salt particle diameter growth and water growth function.

RH (%)	Growth Factor[a]	f(RH)	RH (%)	Growth Factor	f(RH)
1-46	1.0000	1.0000	71	1.8434	3.1269
47	1.5922	2.3584	72	1.8589	3.1729
48	1.6001	2.3799	73	1.8751	3.2055
49	1.6081	2.4204	74	1.8921	3.2459
50	1.6162	2.4488	75	1.9100	3.2673
51	1.6245	2.4848	76	1.9288	3.3478
52	1.6329	2.5006	77	1.9488	3.4174
53	1.6415	2.5052	78	1.9700	3.5202
54	1.6503	2.5279	79	1.9925	3.5744
55	1.6593	2.5614	80	2.0166	3.6329
56	1.6685	2.5848	81	2.0423	3.6905
57	1.6779	2.5888	82	2.0701	3.8080
58	1.6875	2.6160	83	2.1001	3.9505
59	1.6974	2.6581	84	2.1328	4.0398
60	1.7075	2.6866	85	2.1684	4.1127
61	1.7179	2.7341	86	2.2077	4.2824
62	1.7286	2.7834	87	2.2512	4.4940
63	1.7397	2.8272	88	2.2999	4.6078
64	1.7511	2.8287	89	2.3548	4.8573

65	1.7629	2.8594	90	2.4174	5.1165
66	1.7751	2.8943	91	2.4898	5.3844
67	1.7877	2.9105	92	2.5749	5.7457
68	1.8008	2.9451	93	2.6769	6.1704
69	1.8145	3.0105	94	2.8021	6.7178
70	1.8286	3.0485	95	2.9610	7.3492

[a] Diameter at RH/Dry Diameter

REFERENCES

Clegg, S.L.; Brimblecombe, P.; Wexler, A.S., A Thermodynamic Model of the System H^+-NH_4^+-Na^+-SO_4^{2-}-NO^{3-}-Cl^--H_2O at 298.15 K. *J. Phys. Chem.*, **1998**, *102*, 2155-2171.

Lowenthal, D.H.; Kumar, N. $PM_{2.5}$ Mass and Light Extinction Reconstruction in IMPROVE; *J. Air & Waste Manage. Assoc.*, **2003**, *53,* 1109-1120.

Lowenthal, D.H.; Kumar, N. Light Scattering from Sea Salt Aerosols at IMPROVE Sites; *J. Air & Waste Manage. Assoc.*, **2005** (in press).

McInnes, L.M.; Covert, D.S.; Quinn, P.K.; Germani, M.S. Measurements of Chloride Depletion and Sulfur Enrichment in Individual Sea-Salt Particles Collected from the Remote Marine Boundary Layer; *J. Geophys. Res.*, **1994**, *99*, 8257-8268.

Pytkowicz, R.M.; Kester, D.R. The Physical Chemistry of Sea Water; *Oceanogr. Mar. Biol. Ann. Rev.*, **1971**, *9*, 11-60.

Quinn, P.K.; Marshall, S.F.; Bates, T.S.; Covert, D.S.; Kapustin, V.N. Comparison of Measured and Calculated Aerosol Properties Relevant to the Direct Radiative Forcing ot Tropospheric Sulfate Aerosol on Climate. *J. Geophys. Res.*, **1995**, *100*, 8977-8991.

Quinn, P.K.; Kapustin, V.N.; Bates, T.S.; Covert, D.S. Chemical and Optical Properties of Marine Boundary Layer Aerosol Particles of the Mid-Pacific in Relation to Sources and Meteorological Transport; *J. Geophys. Res.*, **1996**, *101*, 6931-6951.

Quinn, P.K.; Coffman, D.J.; Kapustin, V.N.; Bates, T.S.; Covert, D.S. Aerosol Optical Properties in the Marine Boundary Layer During the First Aerosol Characterization Experiment (ACE 1) and the Underlying Chemical and Physcial Aerosol Properties. *J. Geophys. Res.*, **1998**, *103*, 16,547-16,563.

Tang, I.N.; Tridico, A.C.; Fung, K.H. Thermodynamic And Optical Properties of Sea Salt Aerosols; *J. Geophys. Res.*, **1997**, *102*, 23,269-23,275.

USEPA. *Draft Guidance for Tracking Progress Under the Regional Haze Rule*; U.S. Environmental Protection Agency, Office of Air Quality Planning and Standards: Research Triangle Park, NC, September 27, 2001. Available at: Http:/Vista.Cira.Colostate.Edu/IMPROVE/Publications/Guidancedocs/Guidancedocs.Htm.

Organic Mass to Organic Carbon Ratio

A factor of 1.4 is currently used in the "IMPROVE equation" to convert OC to organic mass (OM) to account for unmeasured elements (e.g. O, H, N) in OM. The value of 1.4 was based on an experiment conducted by Grosjean and Friedlander (1975) in urban Pasadena, CA in 1973. They found that the carbon content of these samples averaged 73%. White and Roberts (1977) suggested an OC to OM conversion factor (OM/OC) of 1.4 on the reciprocal of 0.73. Andrews et al. (2000) attempted to explain the reconstructed mass deficit during SEAVS (Southeastern Aerosol and Visibility Study) at Great Smoky Mountains National Park in terms of underestimation of OM.

Turpin and Lim (2001) recommended the use of OM/OC factors of 1.6±0.2 and 2.1 ±0.2 for urban and non-urban aerosol, respectively, based on the chemical structure of organics compounds found in such environments. This is consistent with an expectation that OM/OC ratio should increase as aerosols age during transport and photochemical reactions produce secondary organic compounds that are more oxygenated than their primary precursors. Krivácsy et al. (2001) isolated the polar, water-soluble organic carbon fraction of aerosols from the Jungfraujoch, Switzerland using solid phase extraction. An OM/OC ratio of 1.91 was inferred from elemental composition (C, N, H, and S). Poirot and Husar (2004) found that agreement between reconstructed and measured $PM_{2.5}$ was closer with an OM/OC ratio of 1.8 than with the factor of 1.4 for samples from the IMPROVE and STN networks in the northeastern U.S. during summer, 2002, when large impacts from forest fires in Quebec were observed. Malm et al. (2005) found that $PM_{2.5}$ mass and light scattering closure was achieved assuming an OM/OC ratio of 1.8 during a two-month study at Yosemite National Park in summer, 2002. El-Zanan et al. (2005) derived OM/OC ratios of 1.92±0.40 from solvent extracts of archived filter samples from five IMPROVE sites and 2.07±0.32 from chemical mass balance in 40,532 daily IMPROVE samples at 50 sites from 1988-2003.

While additional experimental work is needed to further explore this issue, it is clear that an OC conversion factor or 1.4 is not applicable for remote U.S. national parks. A consensus value of 1.8 is recommended for use in the proposed new algorithm.

REFERENCES

Andrews, E., Saxena, P., Musarra, S., Hildemann, L.M., Koutrakis, P., McMurry, P.H., Olmez, I., and White, W.H., 2000: Concentration and composition of atmospheric aerosols from the 1995 SEAVS experiment and a review of the closure between chemical and gravimetric measurements. *J. Air & Waste Manage. Assoc*. ***50***, 648-664.

Grosjean, D., and Friedlander, S. K. 1975: Gas-particle distribution factors for organic and other pollutants in the Los Angeles atmosphere. *J. Air Pollut. Control Assoc.*, **25**, 1038-1044.

Krivácsy, Z., Gelencsér, A., Kiss, G., Mézáros, E., Molnár, A., Hoffer, A., Mézáros, T., Sárvári, Z., Temesi, D., Varga, B., Baltensperger, U., Nyeki, S., and Weingartner, E., 2001: Study on the chemical character of water soluble organic compounds in fine atmospheric aerosol at the Jungfraujoch. *J. Atmos. Chem.*, **39**, 235-259.

Malm, W.C., Day, D.E., Carrico, C., Kreidenweis, S.M., Collett, J.L., Jr., McMeeking, G., Lee, and Carillo, J., 2005: Intercomparison and closure calculations using measurements of aerosol species and optical properties during the Yosemite Aerosol Characterization Study, *J. Geophys. Res.*, doi:10.1029/2004JD005494, in press.

Poirot, R.L., and Husar, R.B., 2004: Chemical and physical characteristics of wood smoke in the northeastern U.S. during July 2002: Impacts from Quebec forest fires, Paper #94, A&WMA Specialty Conference: Regional and Global Perspectives on Haze: Causes, Consequences and Controversies, Ashville, NC, October 25-29, 2004.

Turpin, B.J., and Lim, H.-J., 2001: Contributions to $PM_{2.5}$ mass concentrations: revisiting common assumptions for estimating organic mass. *Aerosol. Sci. Technol.,* **35**, 602-610.

White, W. H., and Roberts P. T., 1977: On the nature and origins of visibility-reducing aerosols in the Los Angeles air basin. *Atmos. Environ.*, **11**, 803-812.

Split Component Extinction Efficiency Model

Concentration-Varying Dry Scattering Efficiencies

The current IMPROVE algorithm employs dry scattering efficiencies (E) of 3 m^2/g for ammonium sulfate and ammonium nitrate and 4 m^2/g for organic matter (OM). Data from IMPROVE special studies suggest that dry extinction efficiencies are variable. Lowenthal and Kumar (2005) found that $PM_{2.5}$ mass scattering efficiencies increased with increasing levels of particle light scattering and mass concentration. This was attributed to growth of the dry particle size distribution into size ranges with higher scattering efficiencies under more-polluted conditions, which is related to a higher degree of cloud processing during transport. Malm et al. (2003) estimated dry ammoniated sulfate scattering efficiencies ranging from 2.4-4.1 m^2/g during the Big Bend Aerosol and Visibility Observational Study (BRAVO). A weak relationship between efficiency and ammoniated sulfate mass concentration was reported.

The proposed new IMPROVE algorithm accounts for the increase of ammonium sulfate/ammonium nitrate and organic matter (OM) efficiencies with concentration using a simple mixing model where the concentrations of ammonium sulfate, ammonium nitrate, and OM are each comprised of external mixtures of mass in small and large particle size modes. The large mode represents aged and/or cloud processed particles, while the small mode represents freshly formed particles. These size modes are described by log-normal mass size distributions with geometric mean diameters (D_g) and geometric standard deviations (σ_g) of

0.2 µm and 2.2 for small mode and 0.5 µm and 1.5 for the large mode, respectively. The dry $PM_{2.5}$ scattering efficiencies for small- and large-mode ammonium sulfate (2.2 and 4.8 m^2/g), ammonium nitrate (2.4 and 5.1 m^2/g), and OM (2.8 and 6.1 m^2/g) were calculated using Mie theory at a wavelength of 550 nm based on the log-normal mass size distribution parameters described above. The ammonium sulfate, ammonium nitrate, and OM densities and refractive indexes used in this calculation are 1.77, 1.73, and 1.4 g/cm^3, respectively, and 1.53+i0, 1.55+i0, and 1.55+i0, respectively. No attempt was made to account for possible difference in composition between the two size modes of these particles.

f(RH)

The current IMPROVE algorithm applies a single f(RH) curve to ammonium sulfate and ammonium nitrate scattering which is based on a hygroscopic growth curve ($D_{(RH)}/D_{(Dry)}$) (particle diameter at ambient RH divided by the dry particle diameter) for pure ammonium sulfate that was smoothed between the deliquescence and efflorescence branches (USEPA, 2001). The proposed new IMPROVE algorithm contains f(RH) curves for small- and large-mode ammonium sulfate that are also applied to small and large mode ammonium nitrate. The f(RH) for OM is assumed to be one at all RH for small and large OM modes. The f(RH) for ammonium sulfate and ammonium nitrate are based on the hygroscopic growth curve for pure ammonium sulfate derived from the AIM thermodynamic equilibrium model (Clegg et al., 1998). This growth curve represents the upper branch, also referred to as the efflorescence or hysteresis branch, of the ammonium sulfate growth curve. The upper branch is used because deliquescence is rarely observed in the environment. Because pure ammonium sulfate crystallizes at 37% RH, it is assumed that there is no hygroscopic growth and that the f(RH) is one below this RH.

Dry (RH=0%) light scattering ($b_{sp(Dry)}$) was calculated using Mie theory for small- and large-mode ammonium sulfate. Light scattering at RH = 37-95% at unit RH intervals ($b_{sp(RH)}$) was calculated by applying the AIM ammonium sulfate growth curve to the small and large dry mode size distributions using Mie theory, accounting for the change in particle volume and refractive index from the addition of water. The f(RH), defined as $b_{sp(RH)}/b_{sp(Dry)}$, are listed in Table 9 for the small ($f_{(S)}RH$) and large ($f_{(L)}RH$) modes. Values are presented to RH = 95%, to which higher RH are "rolled back" under the Regional Haze Rule protocol (USEPA, 2001). The same f(RH) are applied to small- and large-mode ammonium sulfate and ammonium nitrate.

Table 9. Water growth for the small and large sized distribution sulfate and nitrate components.

RH (%)	$f_S(RH)$	$f_L(RH)$	RH (%)	$f_S(RH)$	$f_L(RH)$	RH (%)	$f_S(RH)$	$f_L(RH)$
0 to 36	1.00	1.00	**56**	1.78	1.61	**76**	2.60	2.18
37	1.38	1.31	**57**	1.81	1.63	**77**	2.67	2.22
38	1.40	1.32	**58**	1.83	1.65	**78**	2.75	2.27

39	1.42	1.34	**59**	1.86	1.67	**79**	2.84	2.33
40	1.44	1.35	**60**	1.89	1.69	**80**	2.93	2.39
41	1.46	1.36	**61**	1.92	1.71	**81**	3.03	2.45
42	1.48	1.38	**62**	1.95	1.73	**82**	3.15	2.52
43	1.49	1.39	**63**	1.99	1.75	**83**	3.27	2.60
44	1.51	1.41	**64**	2.02	1.78	**84**	3.42	2.69
45	1.53	1.42	**65**	2.06	1.80	**85**	3.58	2.79
46	1.55	1.44	**66**	2.09	1.83	**86**	3.76	2.90
47	1.57	1.45	**67**	2.13	1.86	**87**	3.98	3.02
48	1.59	1.47	**68**	2.17	1.89	**88**	4.23	3.16
49	1.62	1.49	**69**	2.22	1.92	**89**	4.53	3.33
50	1.64	1.50	**70**	2.26	1.95	**90**	4.90	3.53
51	1.66	1.52	**71**	2.31	1.98	**91**	5.35	3.77
52	1.68	1.54	**72**	2.36	2.01	**92**	5.93	4.06
53	1.71	1.55	**73**	2.41	2.05	**93**	6.71	4.43
54	1.73	1.57	**74**	2.47	2.09	**94**	7.78	4.92
55	1.76	1.59	**75**	2.54	2.13	**95**	9.34	5.57

REFERENCES

Clegg, S.L.; Brimblecombe, P.; Wexler, A.S., A Thermodynamic Model of the System H^+-NH_4^+-Na^+-SO_4^{2-}-NO^{3-}-Cl^--H_2O at 298.15 K. *J. Phys. Chem.*, **1998**, *102*, 2155-2171.

Lowenthal, D.H.; Kumar, N., 2004: Variation of Mass Scattering Efficiencies in IMPROVE; *J. Air & Waste Manage. Assoc.*, 2**005**, *54*, 926-934.

Malm, W.C.; Day, D.E.; Kreidenweis, S.M.; Collett, J.L.; Lee, T. Humidity-dependent optical properties of fine particles during the Big Bend Regional Aerosol and Visibility Study. *J. Geophys. Res*., **2003**, *108*, 4279, doi: 10.1029/2002JD002998.

USEPA. *Draft Guidance for Tracking Progress Under the Regional Haze Rule*; U.S. Environmental Protection Agency, Office of Air Quality Planning and Standards: Research Triangle Park, NC, September 27, 2001. Available at: Http:/Vista.Cira.Colostate.Edu/IMPROVE/Publications/Guidancedocs/Guidancedocs.Htm.

Site Specific Rayleigh Scattering

Rayleigh scattering refers to the scattering of light from the molecules of the air, and a constant value of 10 Mm-1 is used in the current IMPROVE algorithm. However, Rayleigh scattering depends on the density of the air and thus varies with temperature and pressure. Site-specific Rayleigh scattering was estimated using a Rayleigh Scattering Calculator developed by Air Resource Specialists, Inc. that calculates Rayleigh scattering as a function of temperature and pressure. For each IMPROVE site, we used the standard U.S. atmospheric pressure corresponding to the monitoring site elevation, and an estimated annual mean temperature. The temperature data were obtained from the nearest

weather stations for time periods encompassing 10 to 30 years and were interpolated to the monitoring site location. Table A2 (at the end of the document) shows the site-specific Rayleigh scattering calculated using this procedure. The recommended integer-rounded site-specific values are shown in the last column of the table. They range from 12Mm^{-1} for sites near sea level to 8Mm^{-1} for sites at about 12,000 feet elevation.

NO_2 Absorption

The NO_2 absorption efficiency term (i.e. 0.33Mm^{-1}/ppm) in the proposed new algorithm is a photopic-weighted absorption efficiency value (PAE_{NO2}). It was calculated by dividing the sum of the products of the relative observer photopic response values ($PR(\lambda)$) for viewing an image of 2° angular size and the spectral NO_2 absorption efficiency values ($AE(\lambda)$) by the sum of the photopic response values, as shown in the equation below.

$$PAE_{NO_2} = \frac{\sum_{350}^{750} PR(\lambda) \times AE(\lambda)}{\sum_{350}^{750} PR(\lambda)}$$

The spectral NO_2 absoption efficiency values are from Dixon (1940) and available in PLUVUE Users Manual (1980), where they were giving in 10ηm increments that were interpolated to generate 1ηm values. The photopic response values are from the CIE Ybar function downloaded directly from the CVRL Color and Vision database. Both are shown in the figure below.

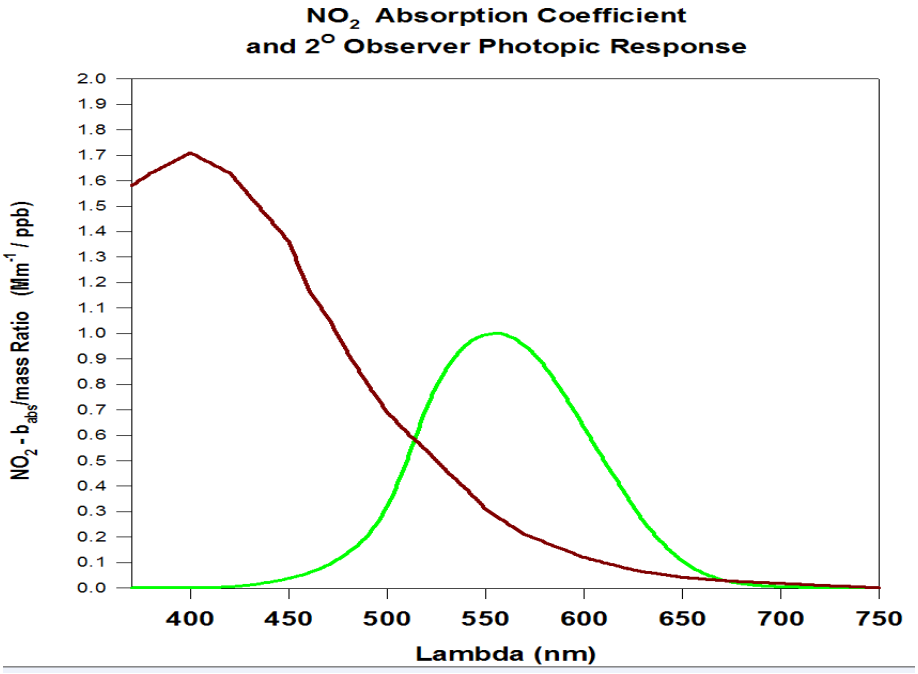

REFERENCES

J.K. Dixon, "The Absorption Coefficient of Nitrogen Dioxide in the Visible Spectrum", Journal of Chemical Physics, Volume 8, February, 1940. pp 157-161

Draft Final Report: User's Manual For The Plume Visibility Model (PLUVUE), July, 1980, Systems Applications, Inc.

CVRL Color & Vision database, CIE (1931) 2-deg color matching function, http://www-cvrl.ucsd.edu/cmfs.htm

Table A1. IMPROVE monitoring sites with nephelometers used to evaluate algorithm performance.

Abbreviation	Name	State
ACAD	Acadia National Park	Maine
BIBE	Big Bend National Park	Texas
BOWA	Boundary Waters Canoe Area	Minnesota
CORI	Columbia River Gorge	Washington
DOSO	Dolly Sods/Otter Creek Wilderness	West Virgina
GICI	Gila Wilderness	New Mexico
GRCA	Grand Canyon National Park	Arizona
GRGU	Great Gulf Wilderness	New Hampshire
GRSM	Great Smoky Mountains	Tennessee
JARB	Jarbidge Wilderness	Nevada
LOPE	Lone Peak Wilderness	Utah
LYBR	Lye Brook Wilderness	Vermont
MACA	Mammoth Cave National Park	Kentucky
MORA	Mount Rainier National Park	Washington
MOZI	Mount Zirkel Wilderness	Colorado
OKEF	Okefenokee National Wildlife Refuge	Florida
SHEN	Shenandoah National Park	Virginia
SHRO	Shining Rock Wilderness	North Carolina
SNAP	Snoqualamie Pass Wilderness	Washington
THIS	Three Sisters Wilderness	Oregon
UPBU	Upper Buffalo Wilderness	Arkansas

Table A2. Site-specific Rayleigh values for all IMPROVE monitoring sites. Revised algorithm uses values rounded to whole integer values (last column).

Monitoring Site Name	Elevation (ft)	Lati-tude	Longi-tude	Standard U.S. Atmo-spher Temp. (C)	Standard U.S. Atmo-sphere Pressure (mb)	Rayleigh at Standard Atmo-sphere (Mm^{-1})	Annual Average Temp. (C)	Corrected Rayleigh (Mm^{-1})	Corrected Rayleigh rounded to integer (Mm^{-1})
Acadia National Park	492	44.4	68.3	14.2	997	11.5	7.4	11.8	12
Addison Pinnacle	1732	42.1	77.2	11.8	951	11.0	7.1	11.2	11
Agua Tibia	1663	33.5	117	11.9	954	11.1	16.7	10.9	11
Arches National Park	5648	38.8	109.6	4	820	9.8	10.0	9.6	10
Arendtsville	879	39.9	77.3	13.5	983	11.3	10.4	11.5	11
Badlands National Park	2414	43.7	101.9	10.4	927	10.8	10.3	10.8	11
Bandelier National Monument	6517	35.8	106.3	2.3	793	9.5	8.7	9.3	9
Big Bend National Park	3526	29.3	103.2	8.2	889	10.5	19.4	10.1	10
Bliss State Park (TRPA)	6940	39	120.1	1.4	780	9.4	4.5	9.3	9
Bondville	692	40.1	88.4	13.8	990	11.4	11.0	11.5	12
Bosque del Apache	4536	33.9	106.9	6.2	855	10.1	14.0	9.9	10
Boundary Waters Canoe Area	1719	47.9	91.5	11.8	952	11.1	2.4	11.4	11
Breton	7	29.1	89.2	15.2	1016	11.7	21.0	11.4	11
Bridger Wilderness	8551	43	109.8	-1.7	734	9.0	2.0	8.8	9
Bridgton	794	44.1	70.7	13.6	986	11.4	6.1	11.7	12
Brigantine National Wildlife Refuge	16	39.5	74.4	15.2	1015	11.6	12.7	11.8	12
Brooklyn Lake	10483	41.4	106.2	-5.6	682	8.4	0.5	8.2	8
Bryce Canyon National Park	8125	37.6	112.2	-0.9	746	9.1	4.1	8.9	9
Cabinet Mountains	4704	48	115.7	5.9	850	10.1	3.2	10.2	10
Cadiz	617	36.8	87.9	14	992	11.4	13.8	11.4	11

Caney Creek	2263	34.5	94.1	10.7	932	10.9	13.1	10.8	11
Canyonlands National Park	5901	38.5	109.8	3.5	812	9.7	11.5	9.4	9
Cape Cod	134	42	70	14.9	1011	11.6	9.8	11.8	12
Cape Romain National Wildlife Refuge	10	32.9	79.7	15.2	1016	11.7	17.9	11.5	12
Capitol Reef (CAPI1)	6199	38.3	111.3	2.9	803	9.6	9.2	9.4	9
Capitol Reef (CARE1)+F76	6199	38.3	111.3	2.9	803	9.6	9.2	9.4	9
Casco Bay	49	43.8	70.1	15.1	1014	11.6	7.6	11.9	12
Chassahowitzka National Wildlife	7	28.7	82.6	15.2	1016	11.7	21.4	11.4	11
Chiricahua National Monument	5150	32	109.4	5	835	9.9	15.5	9.6	10
Cohutta	2437	34.8	84.6	10.4	926	10.8	11.9	10.8	11
Columbia Gorge	738	45.6	122.2	13.7	988	11.4	11.6	11.5	11
Columbia River Gorge	659	45.7	121	13.9	991	11.4	10.5	11.6	12
Connecticut Hill	1656	42.4	76.7	11.9	954	11.1	7.0	11.3	11
Crater Lake National Park	6439	42.9	122.1	2.4	795	9.6	3.2	9.5	10
Craters of the Moon NM(US DOE)	5960	43.5	113.6	3.4	810	9.7	6.2	9.6	10
Death Valley Monument	410	36.5	116.8	14.4	1000	11.5	22.6	11.2	11
Denali National Park	2158	63.7	149	10.9	936	10.9	-3.0	11.5	11
Dolly Sods /Otter Creek Wilderness	3798	39.1	79.4	7.7	879	10.4	6.6	10.4	10
Dome Lands Wilderness	2942	35.7	118.2	9.4	909	10.6	15.0	10.4	10
Dome Lands Wilderness	3034	35.7	118.1	9.2	905	10.6	15.3	10.4	10
Everglades National Park	10	25.4	80.7	15.2	1016	11.7	23.7	11.3	11
Gates of the Mountains	7846	46.8	111.7	-0.4	754	9.2	-1.1	9.2	9
Gila Wilderness	5825	33.2	108.2	3.7	814	9.7	10.6	9.5	10
Glacier National Park	3211	48.5	114	8.8	899	10.6	5.7	10.7	11
Great Basin National Park	6783	39	114.2	1.8	785	9.5	8.8	9.2	9

Great Gulf Wilderness	1460	44.3	71.2	12.3	961	11.1	5.0	11.4	11
Great Sand Dunes National Monument	8213	37.7	105.5	-1.1	744	9.0	6.0	8.8	9
Great Smoky Mountains National Park	2673	35.6	83.9	9.9	918	10.7	11.2	10.7	11
Guadalupe Mountains National Park	5491	31.8	104.8	4.3	825	9.8	15.2	9.5	9
Haleakala National Park	3798	20.8	156.3	7.7	879	10.4	15.0	10.1	10
Hance Camp at Grand Canyon NP	7436	36	112	0.5	766	9.3	6.6	9.1	9
Hawaii Volcanoes National Park	3949	19.4	155.3	7.4	874	10.3	16.3	10.0	10
Hells Canyon	2050	45	116.8	11.1	940	10.9	11.5	10.9	11
Hercules-Glades	1394	36.7	92.9	12.4	964	11.2	13.7	11.1	11
Hillside	4953	34.4	113	5.4	842	10.0	9.9	9.8	10
Hoover	8416	38.1	119.2	-1.5	738	9.0	3.5	8.8	9
Hopi Point #1	7098	36.1	112.2	1.1	776	9.4	7.6	9.1	9
Hopi Point #2 (High Sensitivity)	7098	36.1	112.2	1.1	776	9.4	7.6	9.1	9
Ike's Backbone	4274	34.3	117.9	6.7	864	10.2	14.0	10.0	10
Indian Gardens	3824	36.1	112.1	7.6	879	10.4	16.7	10.0	10
Indian Gardens 2 (High Sensitivity)	3824	36.1	112.1	7.6	879	10.4	16.7	10.0	10
Isle Royale National Park	699	47.9	89.2	14	993	11.4	3.5	11.8	12
Isle Royale National Park (New)	610	47.5	88.1	13.8	989	11.4	3.7	11.9	12
James River Face	981	37.6	79.5	13.3	979	11.3	13.0	11.3	11
Jarbidge Wilderness	6173	41.9	115.4	3	803	9.6	7.1	9.5	9
Jefferson/James River Face Wilderness	918	37.7	79.4	13.4	981	11.3	13.1	11.3	11
Joshua Tree	4028	34.1	116.4	7.2	872	10.3	14.9	10.0	10
Joshua Tree National Monument	4028	34.1	116.4	7.2	872	10.3	14.9	10.0	10
Kaiser	8439	37.2	119.2	-1.5	737	9.0	3.4	8.8	9

Kalmiopsis	295	42.6	124.1	14.6	1005	11.5	13.1	11.6	12
Lassen Volcanic National Park	5756	40.5	121.6	3.8	816	9.8	5.3	9.7	10
Lava Beds	4818	41.7	121.5	5.7	846	10.0	8.7	9.9	10
Linville Gorge	3234	36	81.9	8.8	898	10.5	10.0	10.5	11
Livonia	977	38.5	86.3	13.3	979	11.3	12.2	11.4	11
Lone Peak Wilderness	5799	40.4	111.7	3.7	815	9.7	9.1	9.6	10
Lostwood	2270	48.6	102.4	10.7	932	10.9	3.2	11.2	11
Lye Brook Wilderness	3300	43.1	73.1	8.7	896	10.5	2.4	10.8	11
Lynden	92	49	122.6	15	1013	11.6	10.1	11.8	12
M.K. Goddard	1269	41.4	80.1	12.7	968	11.2	9.0	11.4	11
Mammoth Cave National Park	813	37.1	86.1	13.6	985	11.4	13.7	11.4	11
Mauna Loa National Observatory (MALO1)	11152	19.5	155.6	-6.9	665	8.3	7.0	7.9	8
Meadview	2959	36	114.1	9.3	908	10.6	16.2	10.4	10
Medicine Lake	1984	48.5	104.5	11.3	942	11.0	4.8	11.2	11
Mesa Verde National Park	7141	37.2	108.5	1	774	9.4	8.7	9.1	9
Mingo	367	37	90.1	14.5	1002	11.5	14.3	11.5	12
Mohawk Mt.	1745	41.8	73.3	11.7	951	11.0	6.3	11.3	11
Monture	4241	47.1	113.2	6.8	865	10.2	3.5	10.3	10
Moosehorn NWR	308	45.1	67.3	14.6	1004	11.5	6.0	11.9	12
Mount Baldy	8243	34.1	109.4	-1.1	743	9.0	7.6	8.8	9
Mount Hood	4398	45.3	121.8	6.5	860	10.2	4.3	10.3	10
Mount Rainier National Park	1401	46.8	122.1	12.4	963	11.2	8.9	11.3	11
Mount Zirkel Wilderness	10637	40.5	106.7	-5.9	678	8.4	0.2	8.2	8
Mount Zirkel Wilderness (Storm Peak)	10562	40.5	106.7	-5.7	680	8.4	0.5	8.2	8
North Absaroka	8134	44.7	109.4	-0.9	746	9.1	-0.9	9.1	9
North Cascades	1889	48.7	121.1	11.5	946	11.0	7.2	11.2	11

Okefenokee National Wildlife Refuge	161	30.7	82.1	14.9	1010	11.6	20.3	11.4	11
Old Town	213	44.9	68.6	14.8	1008	11.6	6.2	11.9	12
Olympic	1968	48	123	11.3	943	11.0	10.9	11.0	11
Organ Pipe	1847	32	113	11.5	947	11.0	21.0	10.7	11
Pasayten	5360	48.4	119.9	4.6	829	9.9	4.8	9.9	10
Petrified Forest National Park	5796	35.1	109.8	3.7	815	9.7	11.7	9.5	9
Phoenix	1109	33.5	112.1	13	974	11.3	23.4	10.9	11
Pinnacles National Monument	1040	36.5	121.2	13.1	980	11.3	16.0	11.2	11
Point Reyes National Seashore	279	38.1	122.9	14.6	1005	11.6	11.3	11.7	12
Presque Isle	535	46.7	68	14.1	996	11.5	4.8	11.8	12
Proctor Maple R. F.	1322	44.5	72.9	12.6	966	11.2	4.5	11.5	12
Puget Sound	262	47.6	122.3	14.7	1006	11.6	10.7	11.7	12
Quabbin Summit	1033	42.3	72.3	13.2	977	11.3	6.7	11.6	12
Quaker City	1233	39.9	81.3	12.8	970	11.2	9.8	11.3	11
Queen Valley	2158	33.3	111.3	10.9	936	10.9	21.8	10.5	11
Redwood National Park	804	41.6	124.1	13.6	985	11.4	8.7	11.6	12
Rocky Mountain National Park	9036	40.3	105.5	-2.7	721	8.8	1.9	8.7	9
Rocky Mountain National Park (Headquarters)	7872	40.4	105.6	-0.4	753	9.1	5.5	8.9	9
Saguaro National Monument	3060	32.2	110.7	9.1	904	10.6	18.1	10.3	10
Saguaro West	2355	32.2	111.2	10.5	929	10.8	21.5	10.4	10
Salmon National Forest	9145	45.2	114	-2.9	718	8.8	-7.6	8.9	9
Salt Creek	3533	33.5	104.4	8.2	888	10.5	15.3	10.2	10
San Andres	4674	32.7	106.5	5.9	851	10.1	13.3	9.8	10
San Gabriel	5874	34.3	118	3.6	813	9.7	13.1	9.4	9
San Gorgonio Wilderness	5592	34.2	116.9	4.1	821	9.8	12.0	9.5	10

San Pedro Parks	9574	36	106.8	-3.8	706	8.7	-0.3	8.6	9
San Rafael	3126	34.7	120	9	902	10.6	16.7	10.3	10
Sawtooth National Forest	6494	44.2	114.9	2.3	794	9.5	1.1	9.6	10
Scoville	4920	43.7	113	5.4	843	10.0	6.1	10.0	10
Seney	708	46.3	85.9	13.8	989	11.4	5.8	11.7	12
Sequoia National Park	1755	36.5	118.8	11.7	950	11.0	17.0	10.8	11
Shenandoah National Park	3601	38.5	78.4	8.1	886	10.4	8.2	10.4	10
Shining Rock Wilderness	5317	35.4	82.8	4.7	830	9.9	7.4	9.8	10
Sierra Ancha	5232	34.1	110.9	4.8	833	9.9	12.5	9.7	10
Sikes	148	32.1	92.4	14.9	1010	11.6	18.2	11.5	11
Simeonof	98	55.3	160.5	15	1012	11.6	4.5	12.1	12
Sipsy Wilderness	915	34.3	87.3	13.4	981	11.3	15.5	11.2	11
Snoqualamie Pass, Snoqualamie N.F	3805	47.4	121.4	7.7	879	10.4	3.2	10.5	11
South Lake Tahoe	6232	38.9	120	2.8	802	9.6	6.1	9.5	10
Spokane Res.	1797	47.9	117.9	11.6	949	11.0	10.0	11.1	11
St. Marks	7	30.1	84.2	15.2	1016	11.7	19.8	11.5	11
Starkey	4126	45.2	118.5	7	869	10.3	4.2	10.4	10
Sula (Selway Bitteroot Wilderness)	6242	45.9	114	2.8	801	9.6	-0.5	9.7	10
Swanquarter	7	35.5	76.2	15.2	1016	11.7	16.9	11.6	12
Sycamore Canyon	6691	35.1	112	1.9	788	9.5	9.8	9.2	9
Theodore Roosevelt	2798	46.9	103.4	9.7	914	10.7	5.1	10.9	11
Three Sisters Wilderness	2903	44.3	122	9.4	910	10.7	6.8	10.8	11
Tonto National Monument	2578	33.6	111.1	10.1	921	10.8	18.7	10.4	10
Trapper Creek	479	62.3	150.3	14.3	998	11.5	2.3	12.0	12
Trinity	3303	40.8	122.8	8.7	896	10.5	12.9	10.4	10
Tuxedni	33	60	152.6	15.1	1015	11.6	1.8	12.2	12
UL Bend	2929	47.6	108.7	9.4	909	10.6	5.2	10.8	11

Upper Buffalo Wilderness	2371	35.8	93.2	10.5	928	10.8	12.5	10.8	11
Virgin Islands National Park	210	18.3	64.8	14.8	1008	11.6	26.1	11.1	11
Voyageurs National Park 1	1138	48.6	93.2	12.9	973	11.3	3.1	11.7	12
Voyageurs National Park 2	1407	48.4	92.8	12.4	963	11.2	2.6	11.6	12
Washington D.C.	52	38.9	77	15.1	1014	11.6	14.5	11.7	12
Weminuche Wilderness	9069	37.7	107.8	-2.8	720	8.8	1.5	8.7	9
Wheeler Peak	11060	36.6	105.5	-6.7	667	8.3	-3.0	8.2	8
White Mountain	6724	33.5	105.5	1.9	787	9.5	9.9	9.2	9
White Pass	6002	46.6	121.4	3.3	809	9.7	1.4	9.8	10
White River National Forest	11211	39.2	106.8	-7	663	8.2	-0.3	8.0	8
Wichita Mountains	1699	34.7	98.7	11.8	952	11.1	15.7	10.9	11
Wind Cave	4264	43.6	103.5	6.7	864	10.2	8.1	10.2	10
Yellowstone National Park 1	7744	44.6	110.4	-0.1	757	9.2	-0.2	9.2	9
Yellowstone National Park 2	7954	44.6	110.4	-0.6	751	9.1	-0.8	9.1	9
Yosemite National Park	5297	37.7	119.7	4.7	831	9.9	8.0	9.8	10
Zion	5068	37.5	113.2	5.2	838	10.0	13.2	9.7	10

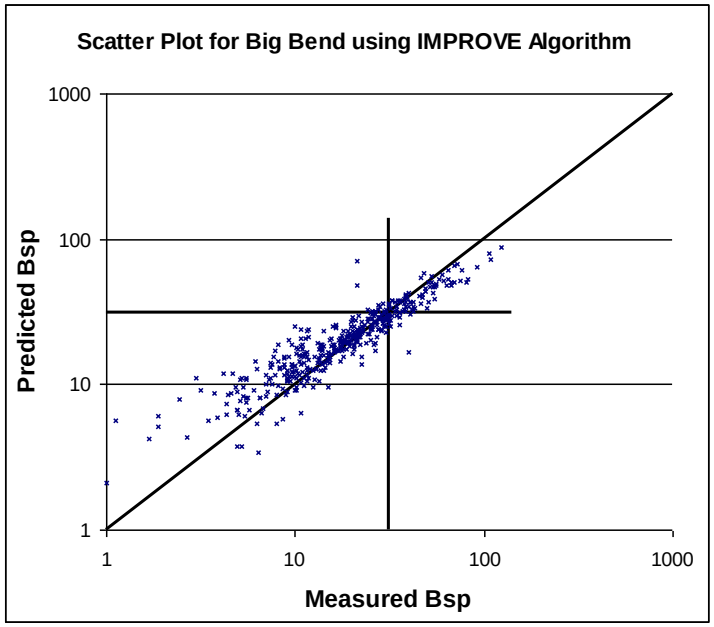
Scatter Plot for Big Bend using IMPROVE Algorithm
Predicted Bsp
Measured Bsp
1000
100
10
1
1
10
100
1000

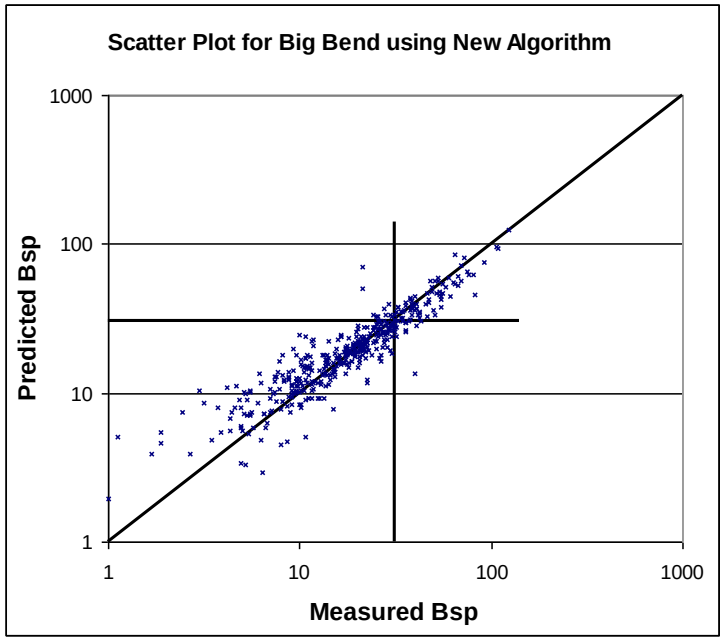
Scatter Plot for Big Bend using New Algorithm
Predicted Bsp
Measured Bsp
1000
100
10
1
1
10
100
1000

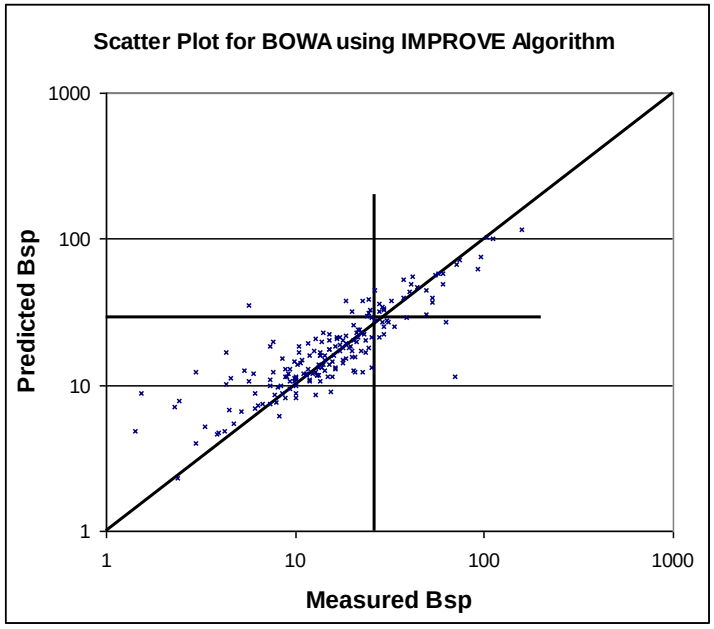
Scatter Plot for BOWA using IMPROVE Algorithm
Predicted Bsp
Measured Bsp
1000
100
10
1
1
10
100
1000

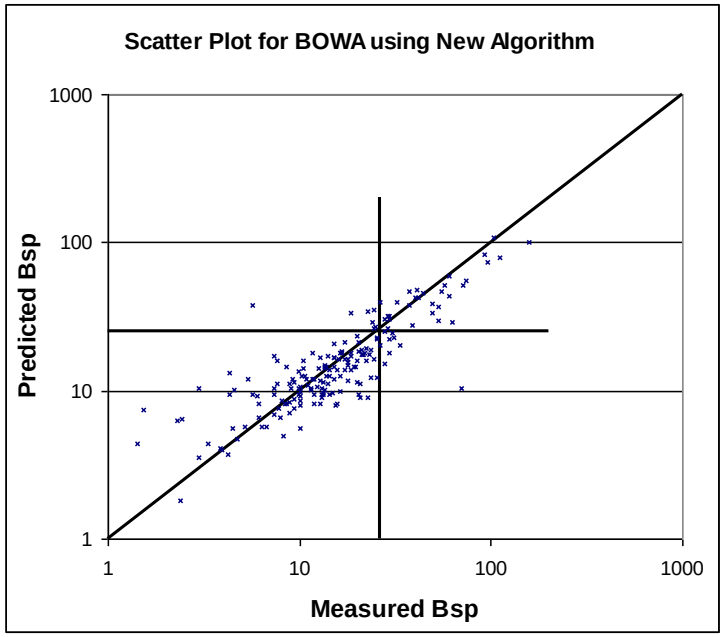
Scatter Plot for BOWA using New Algorithm
Predicted Bsp
Measured Bsp
1000
100
10
1
1
10
100
1000

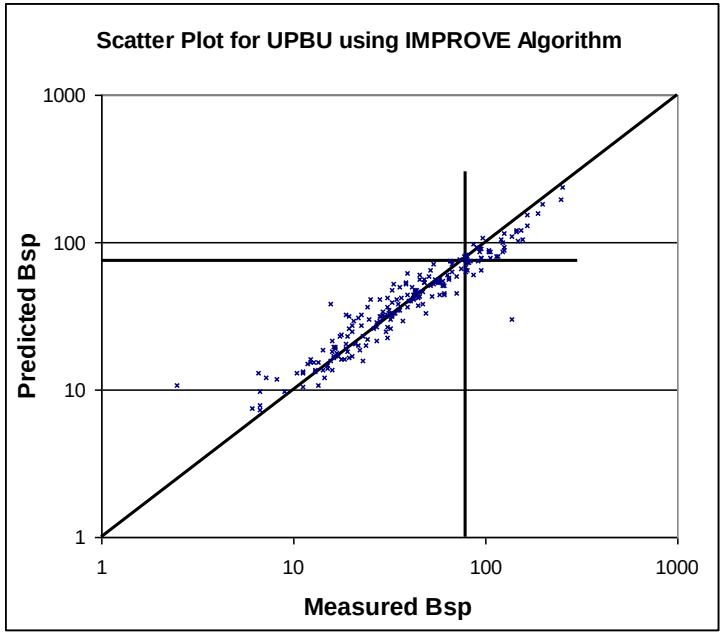
Scatter Plot for UPBU using IMPROVE Algorithm
Predicted Bsp
Measured Bsp
1000
100
10
1
1
10
100
1000

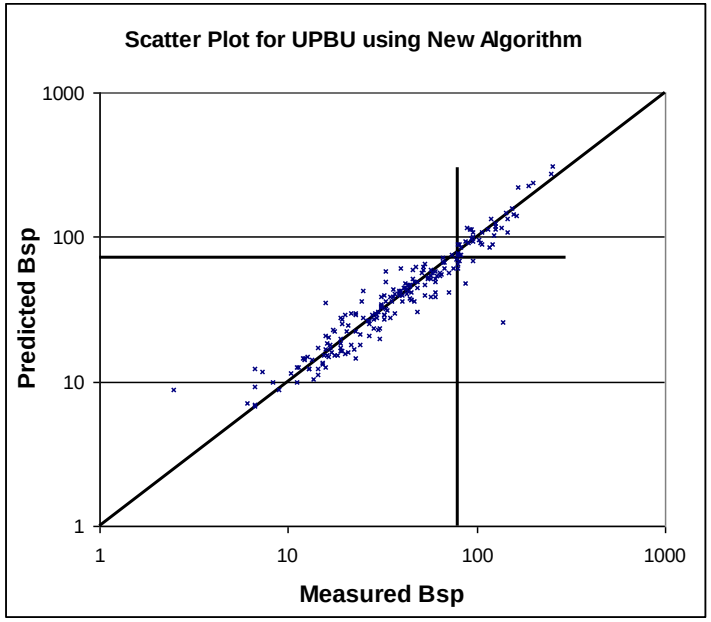
Scatter Plot for UPBU using New Algorithm
Predicted Bsp
Measured Bsp
1000
100
10
1
1
10
100
1000

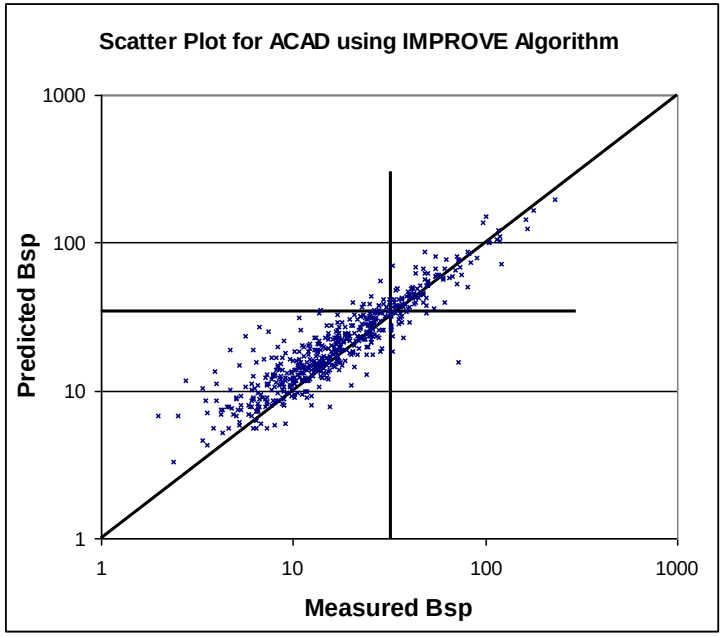
Scatter Plot for ACAD using IMPROVE Algorithm
Predicted Bsp
Measured Bsp
1000
100
10
1
1
10
100
1000

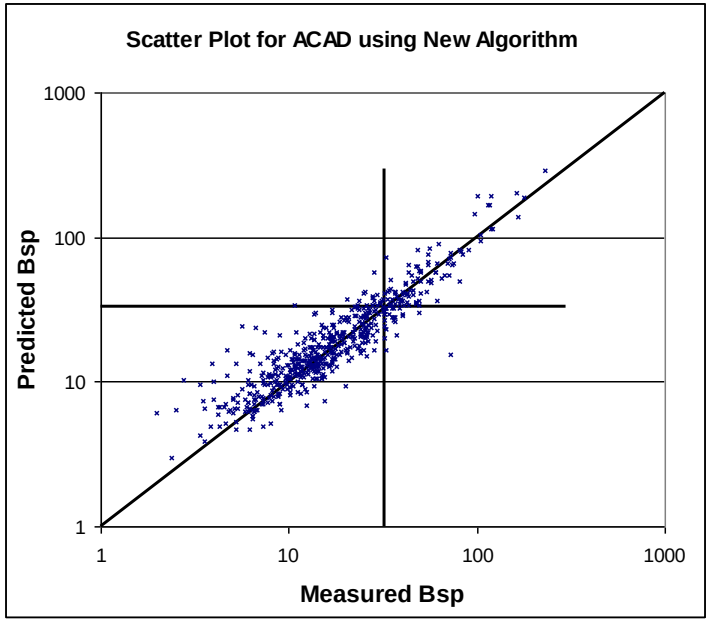
Scatter Plot for ACAD using New Algorithm
Predicted Bsp
Measured Bsp
1000
100
10
1
1
10
100
1000

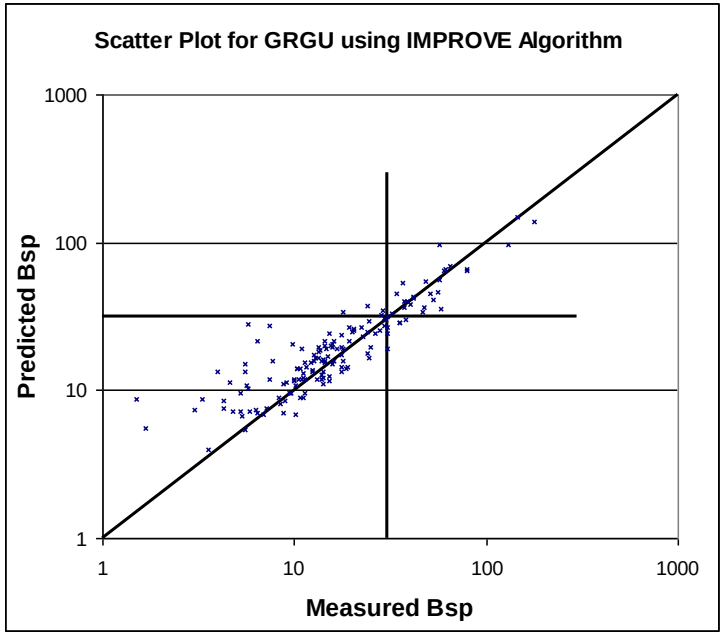
Scatter Plot for GRGU using IMPROVE Algorithm
Predicted Bsp
Measured Bsp
1000
100
10
1
1
10
100
1000

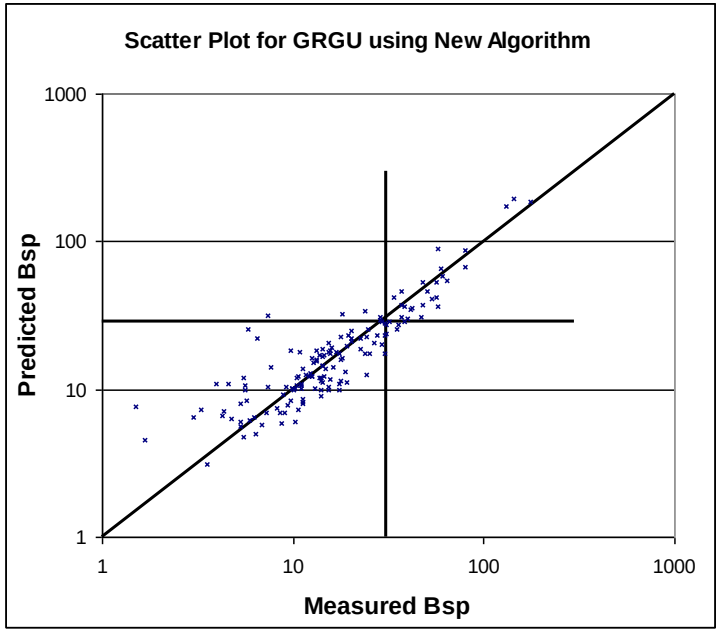
Scatter Plot for GRGU using New Algorithm
Predicted Bsp
Measured Bsp
1000
100
10
1
1
10
100
1000

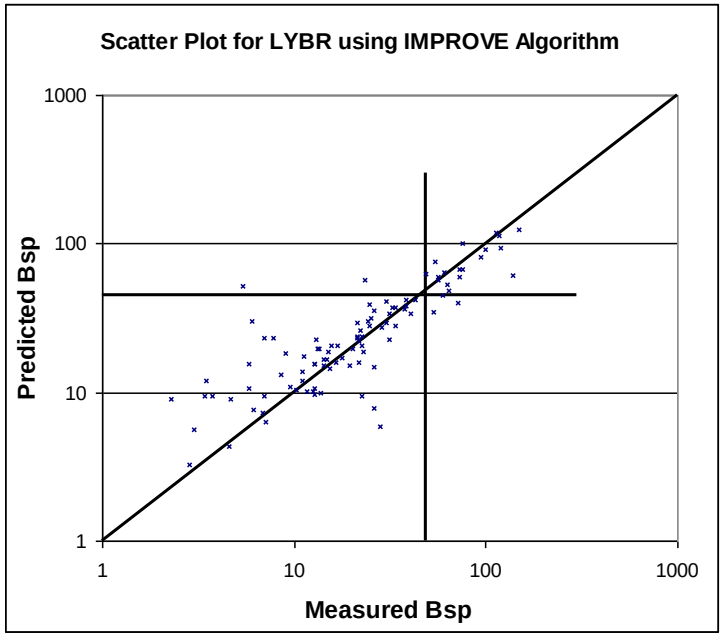
Scatter Plot for LYBR using IMPROVE Algorithm
Predicted Bsp
Measured Bsp
1000
100
10
1
1
10
100
1000

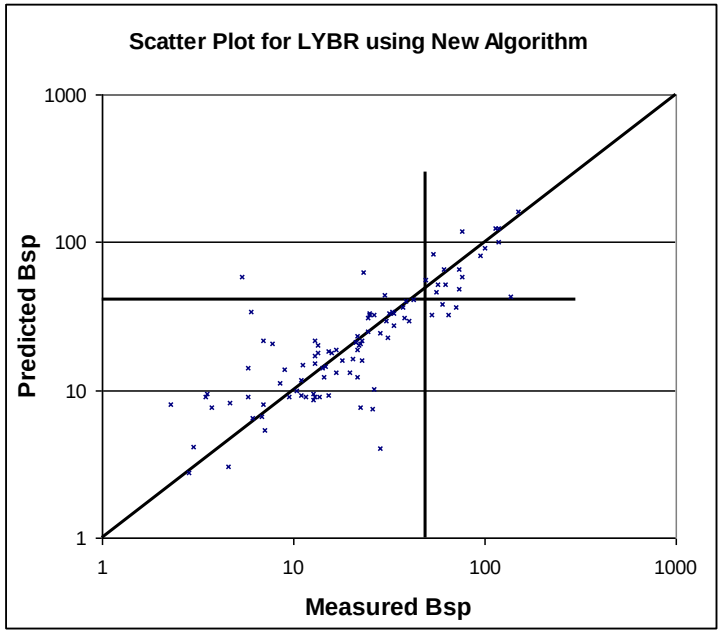
Scatter Plot for LYBR using New Algorithm
Predicted Bsp
Measured Bsp
1000
100
10
1
1
10
100
1000

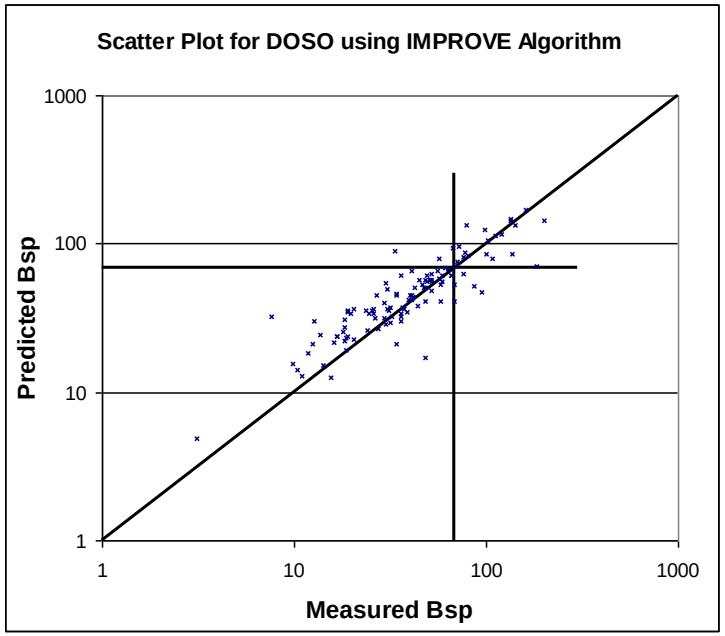
Scatter Plot for DOSO using IMPROVE Algorithm
Predicted Bsp
Measured Bsp
1000
100
10
1
1
10
100
1000

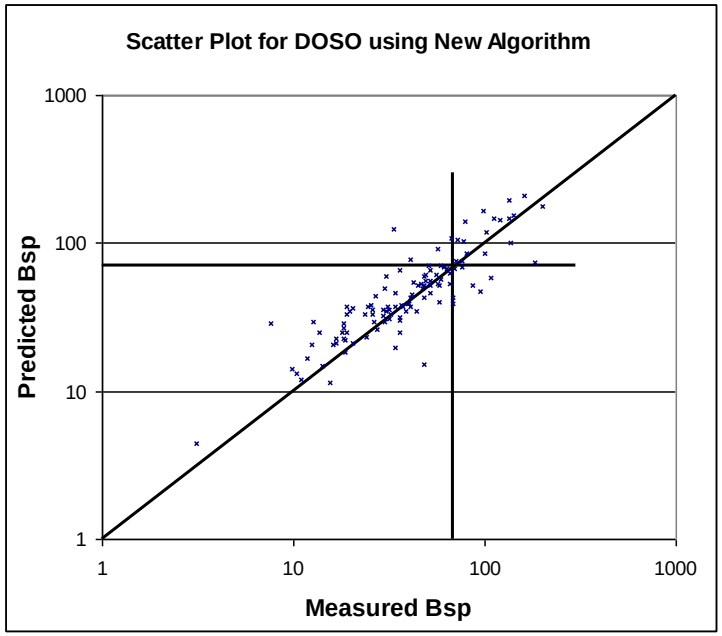
Scatter Plot for DOSO using New Algorithm
Predicted Bsp
Measured Bsp
1000
100
10
1
1
10
100
1000

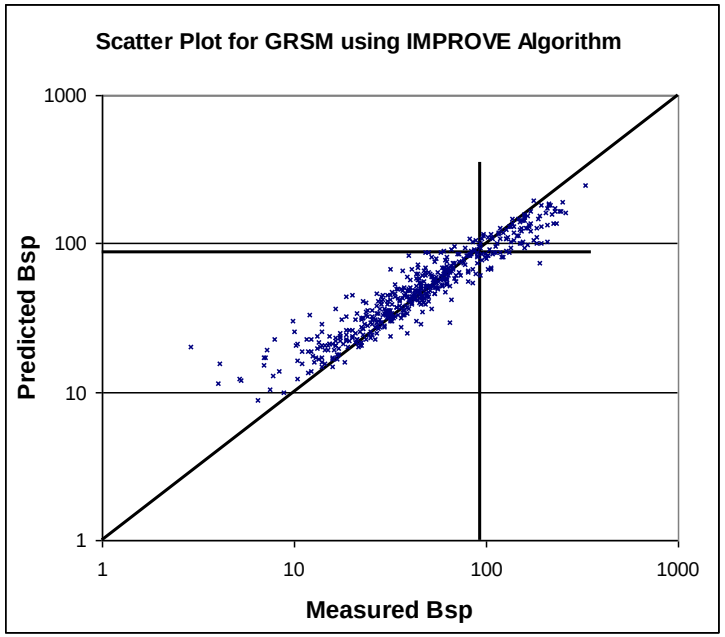
Scatter Plot for GRSM using IMPROVE Algorithm
Predicted Bsp
Measured Bsp
1000
100
10
1
1
10
100
1000

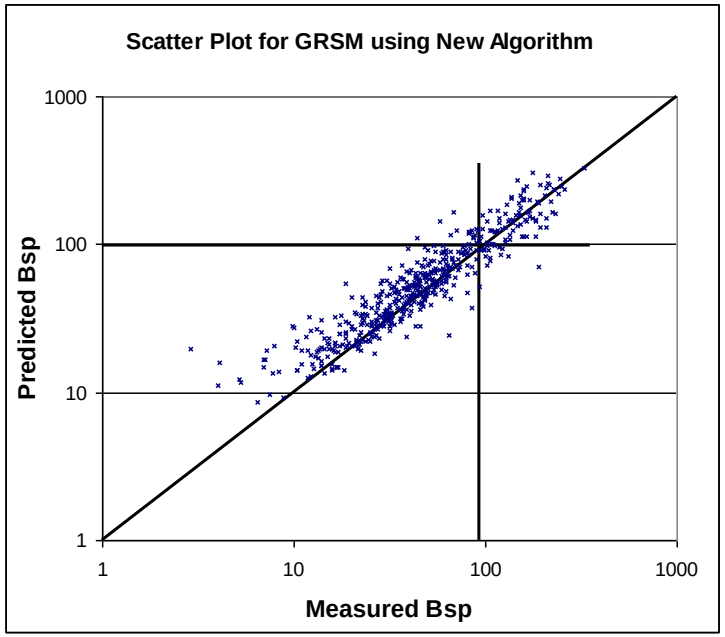
Scatter Plot for GRSM using New Algorithm
Predicted Bsp
Measured Bsp
1000
100
10
1
1
10
100
1000

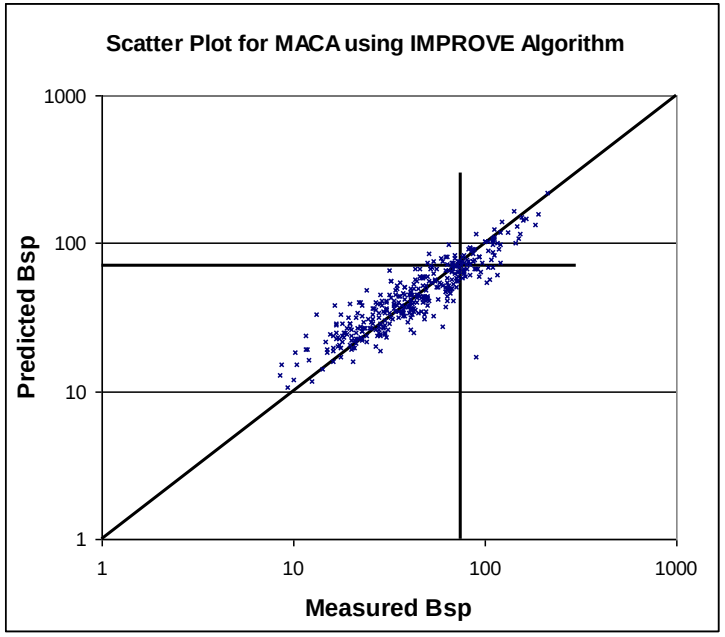
Scatter Plot for MACA using IMPROVE Algorithm
Predicted Bsp
Measured Bsp
1000
100
10
1
1
10
100
1000

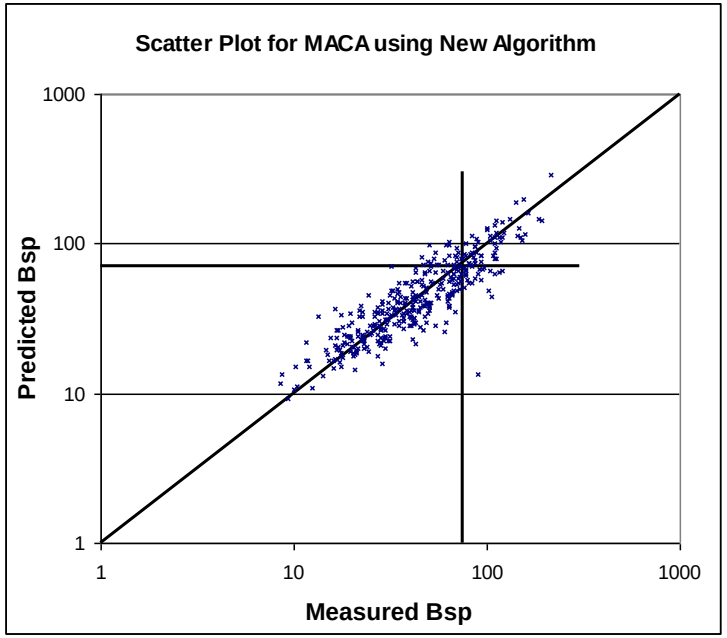
Scatter Plot for MACA using New Algorithm
Predicted Bsp
Measured Bsp
1000
100
10
1
1
10
100
1000

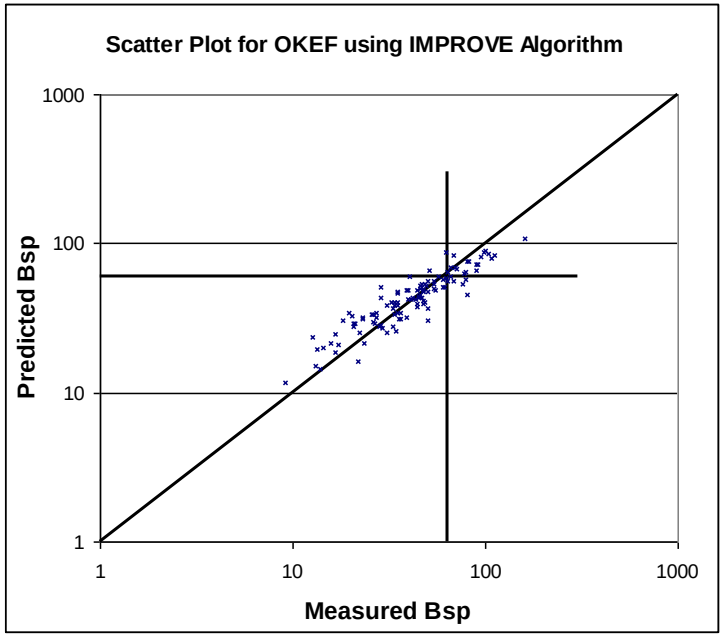
Scatter Plot for OKEF using IMPROVE Algorithm
Predicted Bsp
Measured Bsp
1000
100
10
1
1
10
100
1000

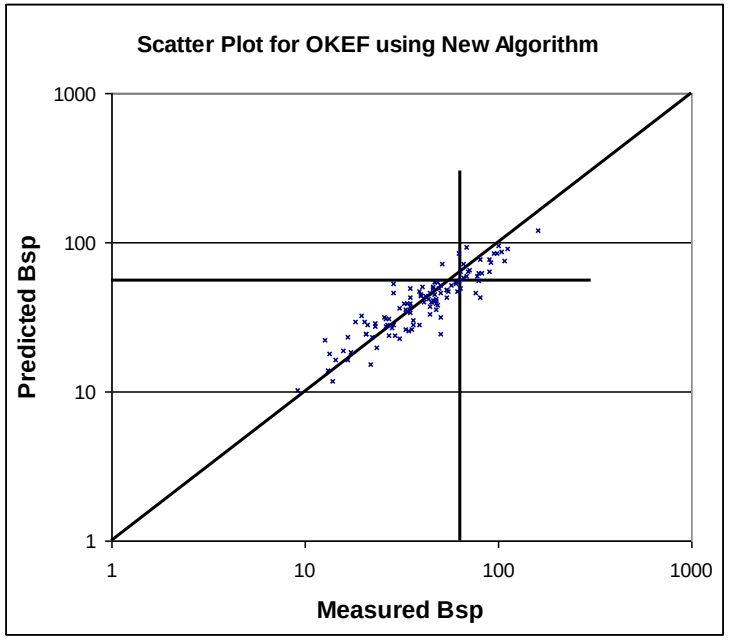
Scatter Plot for OKEF using New Algorithm
Predicted Bsp
Measured Bsp
1000
100
10
1
1
10
100
1000

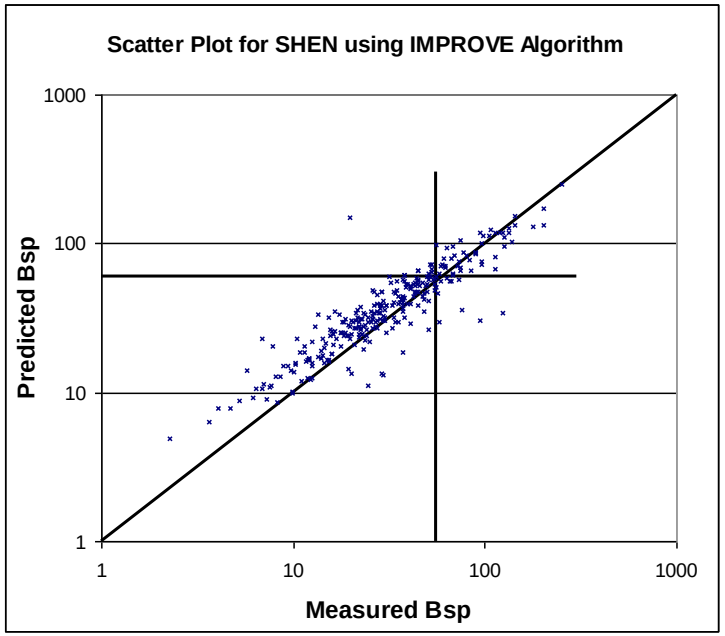
Scatter Plot for SHEN using IMPROVE Algorithm
Predicted Bsp
Measured Bsp
1000
100
10
1
1
10
100
1000

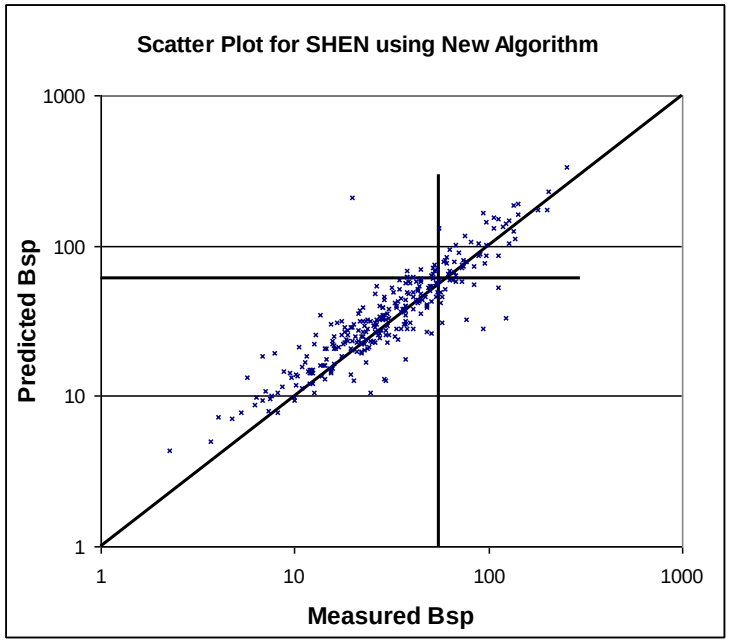
Scatter Plot for SHEN using New Algorithm
Predicted Bsp
Measured Bsp
1000
100
10
1
1
10
100
1000

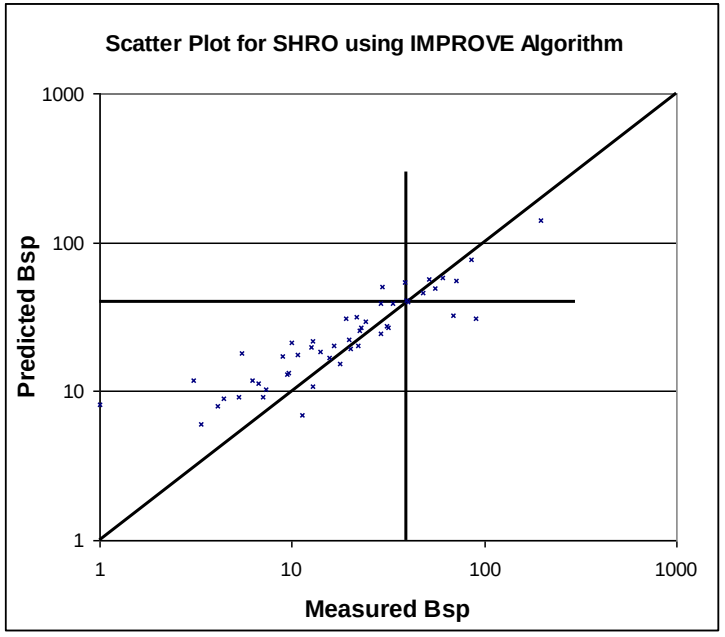
Scatter Plot for SHRO using IMPROVE Algorithm
Predicted Bsp
Measured Bsp
1000
100
10
1
1
10
100
1000

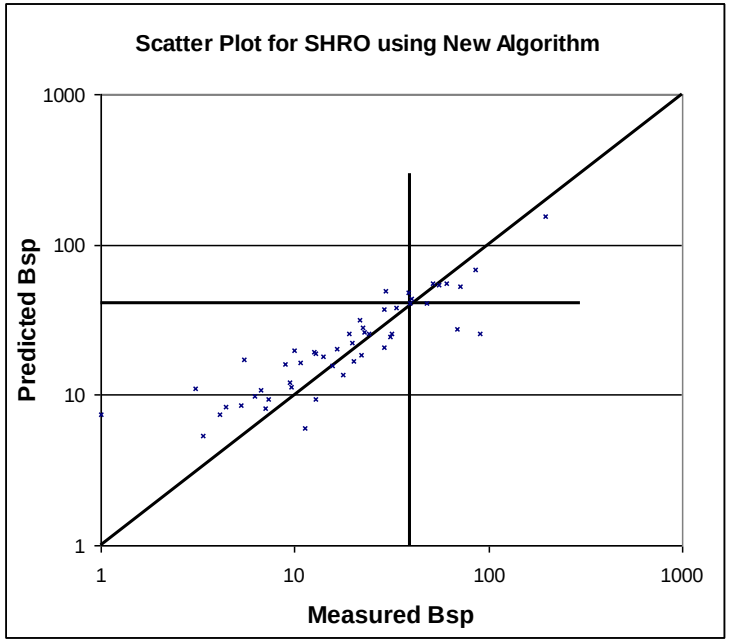
Scatter Plot for SHRO using New Algorithm
Predicted Bsp
Measured Bsp
1000
100
10
1
1
10
100
1000

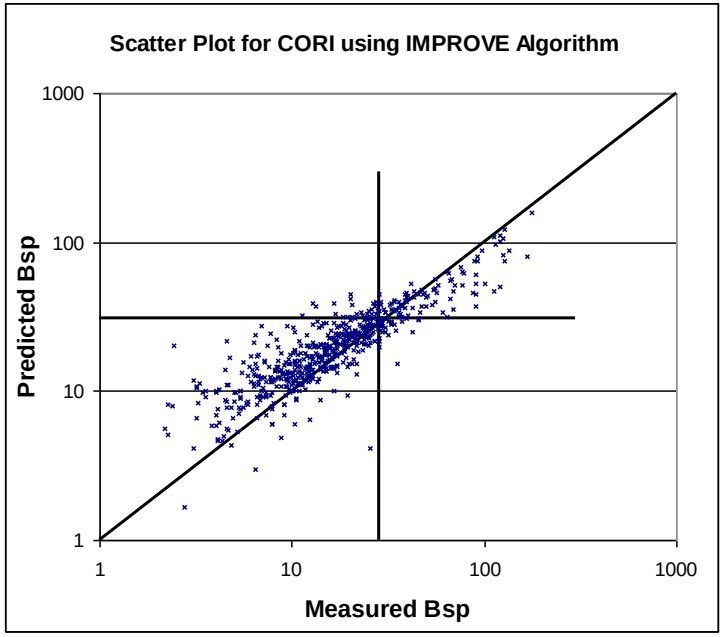
Scatter Plot for CORI using IMPROVE Algorithm
Predicted Bsp
Measured Bsp
1000
100
10
1
1
10
100
1000

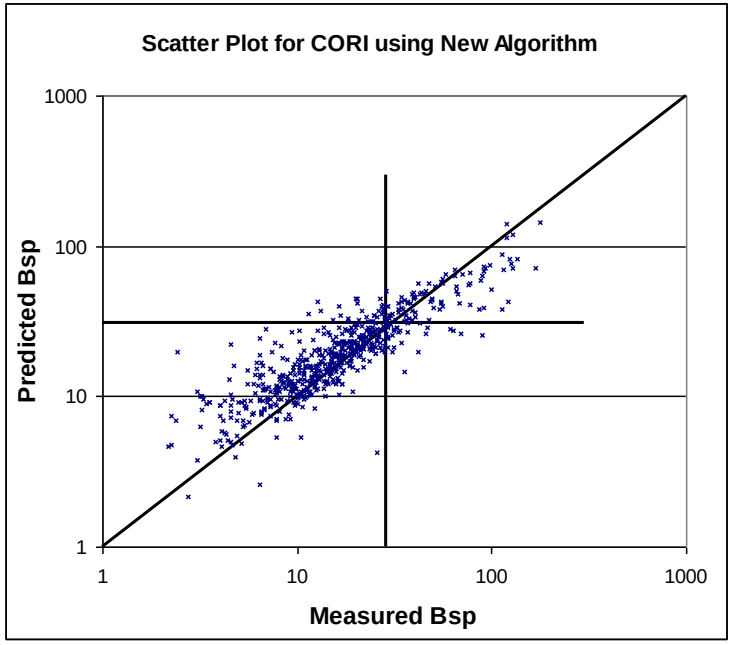
Scatter Plot for CORI using New Algorithm
Predicted Bsp
Measured Bsp
1000
100
10
1
1
10
100
1000

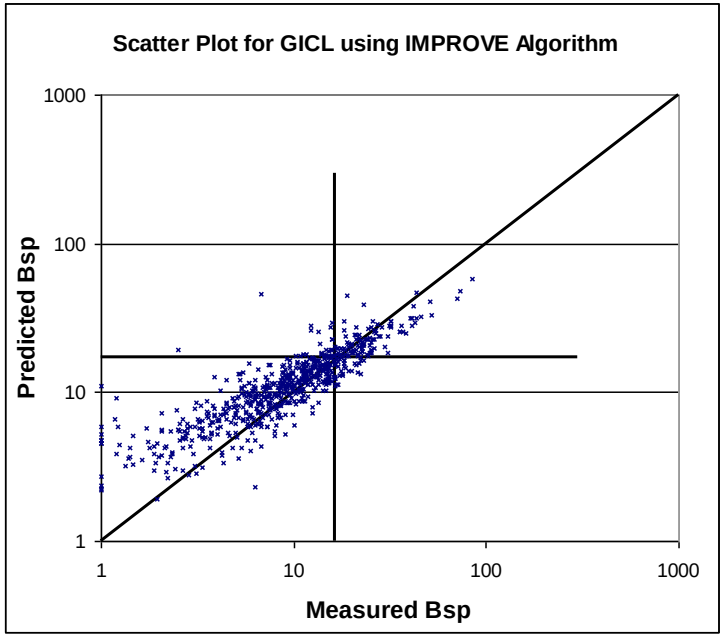
Scatter Plot for GICL using IMPROVE Algorithm
Predicted Bsp
Measured Bsp
1000
100
10
1
1
10
100
1000

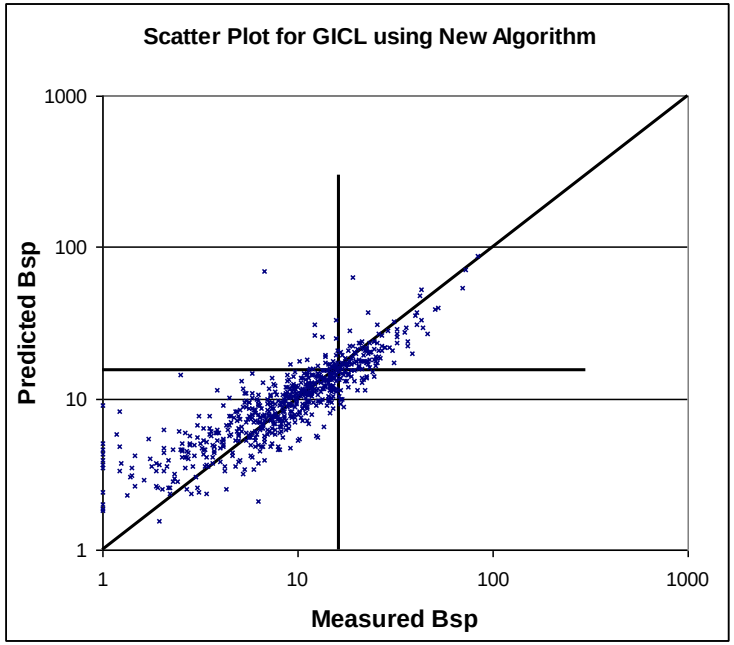
Scatter Plot for GICL using New Algorithm
Predicted Bsp
Measured Bsp
1000
100
10
1
1
10
100
1000

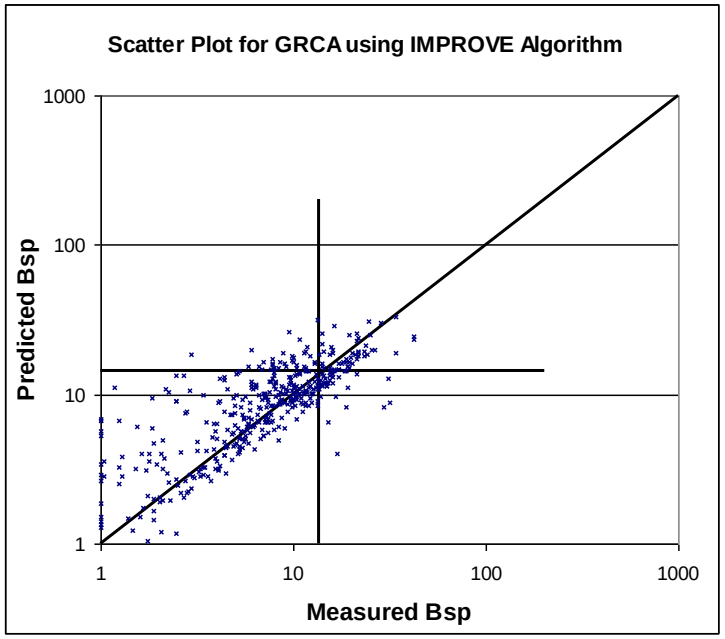
Scatter Plot for GRCA using IMPROVE Algorithm
Predicted Bsp
Measured Bsp
1000
100
10
1
1
10
100
1000

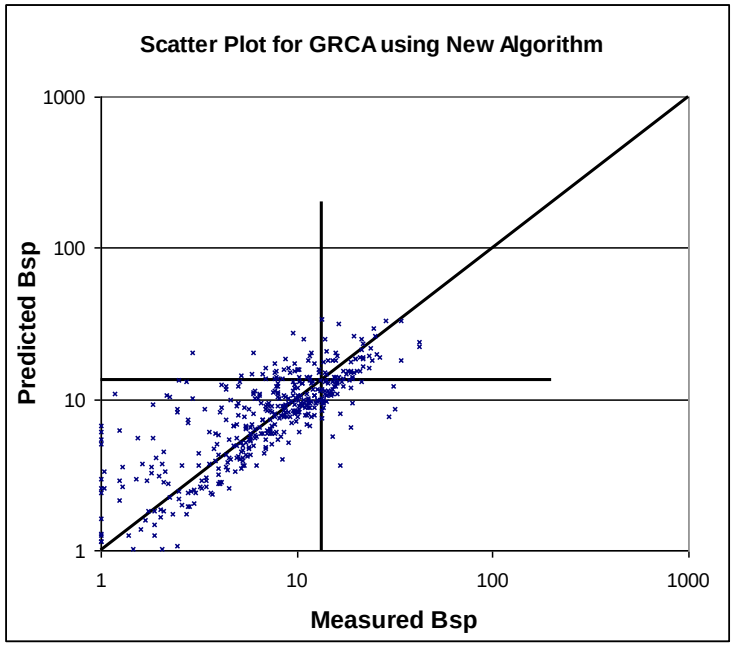
Scatter Plot for GRCA using New Algorithm
Predicted Bsp
Measured Bsp
1000
100
10
1
1
10
100
1000

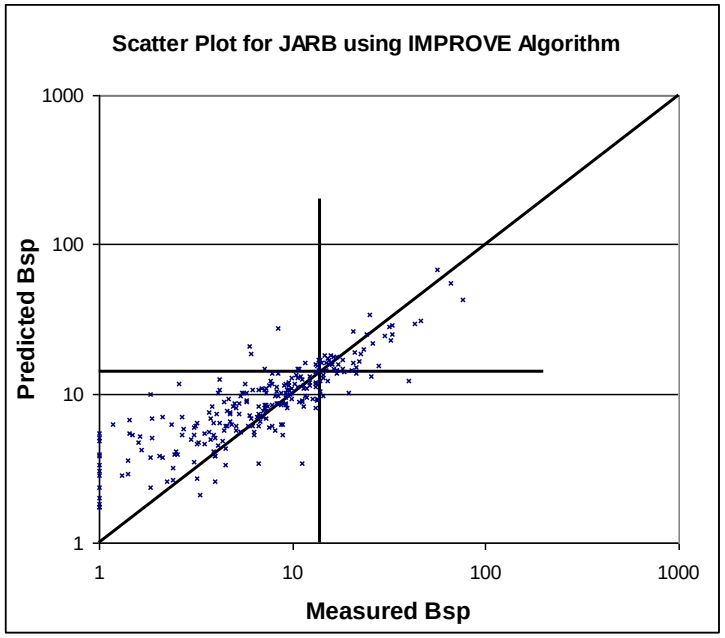
Scatter Plot for JARB using IMPROVE Algorithm
Predicted Bsp
Measured Bsp
1000
100
10
1
1
10
100
1000

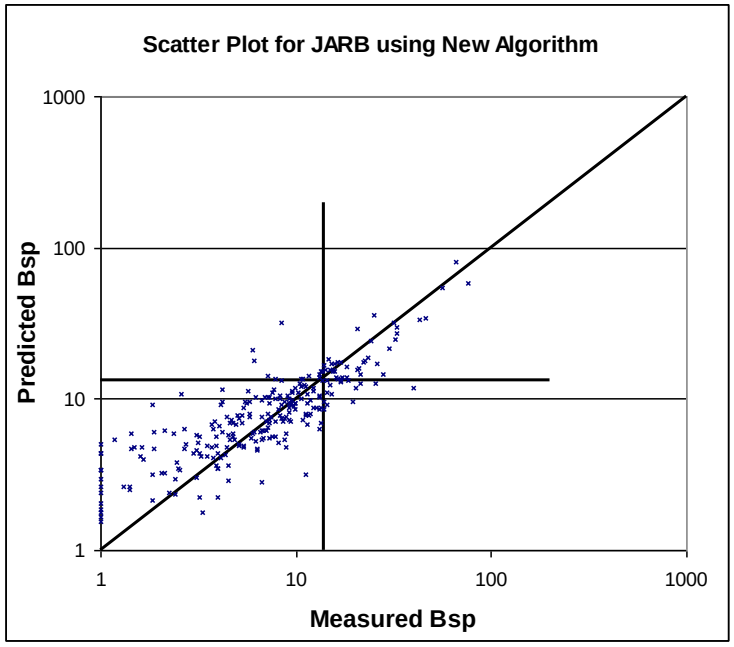
Scatter Plot for JARB using New Algorithm
Predicted Bsp
Measured Bsp
1000
100
10
1
1
10
100
1000

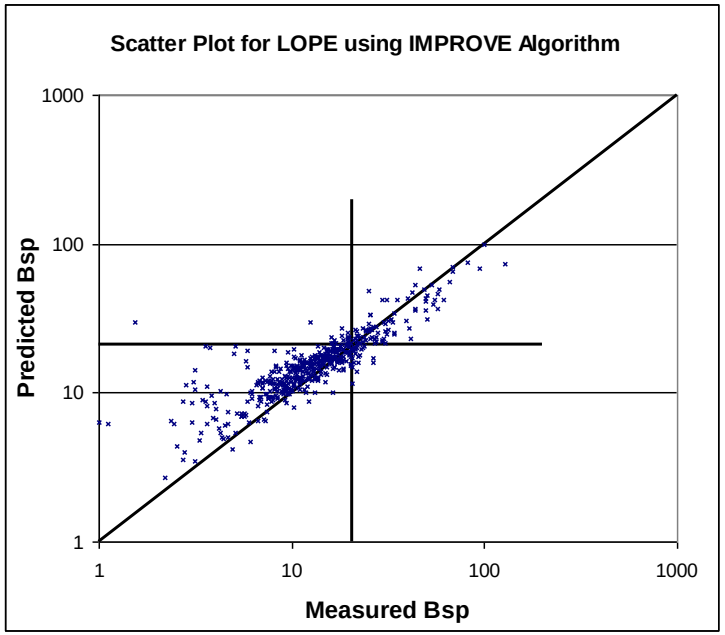
Scatter Plot for LOPE using IMPROVE Algorithm
Predicted Bsp
Measured Bsp
1000
100
10
1
1
10
100
1000

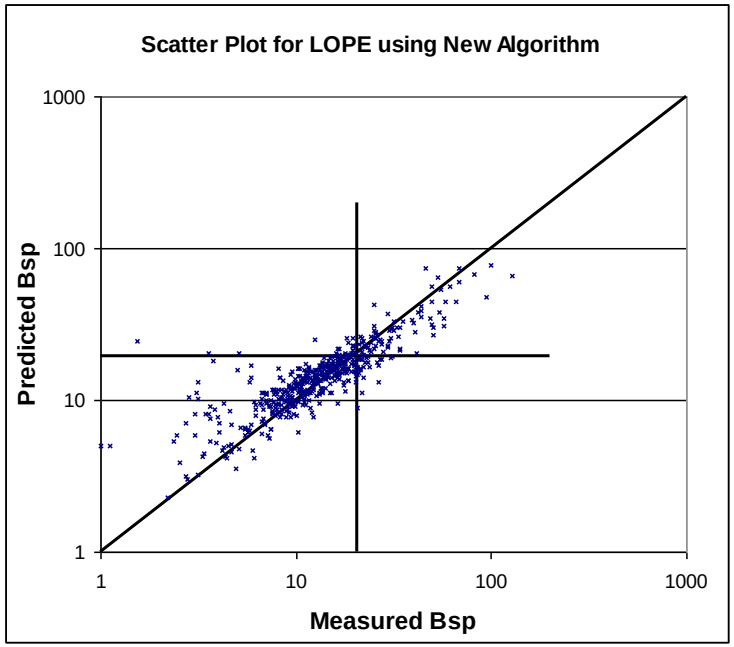
Scatter Plot for LOPE using New Algorithm
Predicted Bsp
Measured Bsp
1000
100
10
1
1
10
100
1000

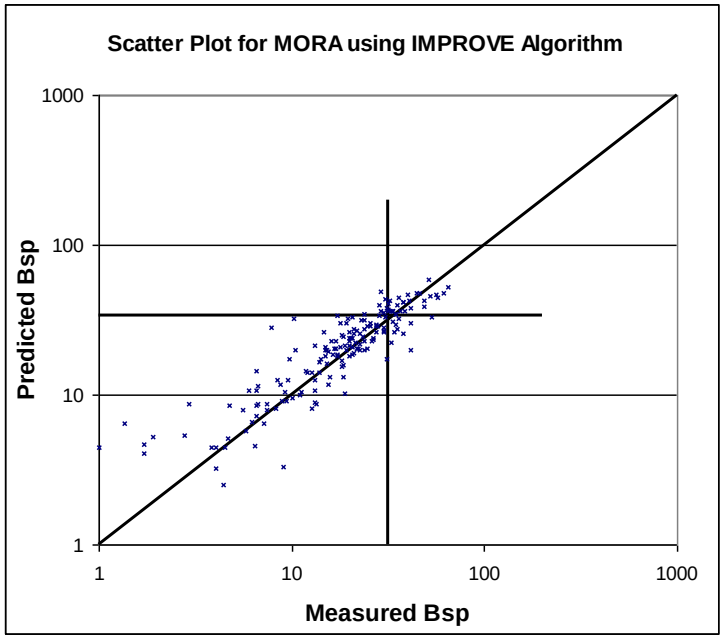
Scatter Plot for MORA using IMPROVE Algorithm
Predicted Bsp
Measured Bsp
1000
100
10
1
1
10
100
1000

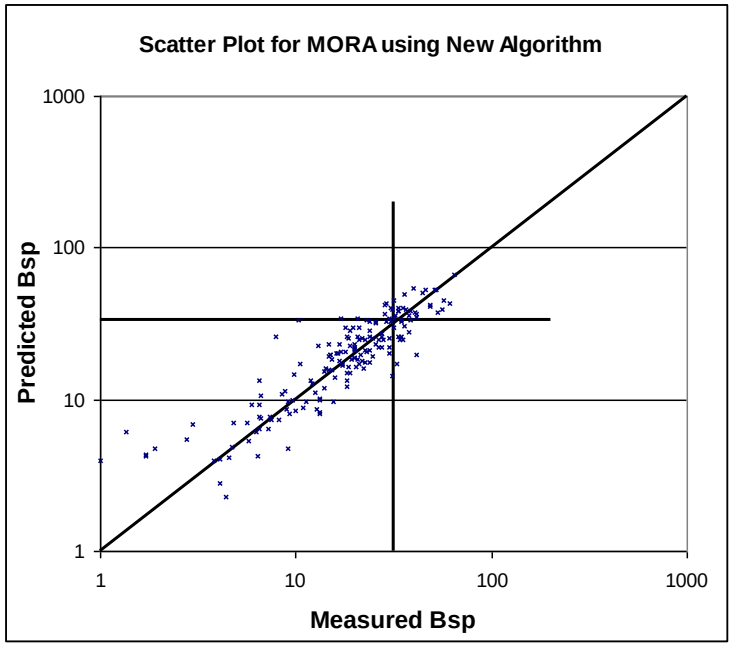
Scatter Plot for MORA using New Algorithm
Predicted Bsp
Measured Bsp
1000
100
10
1
1
10
100
1000

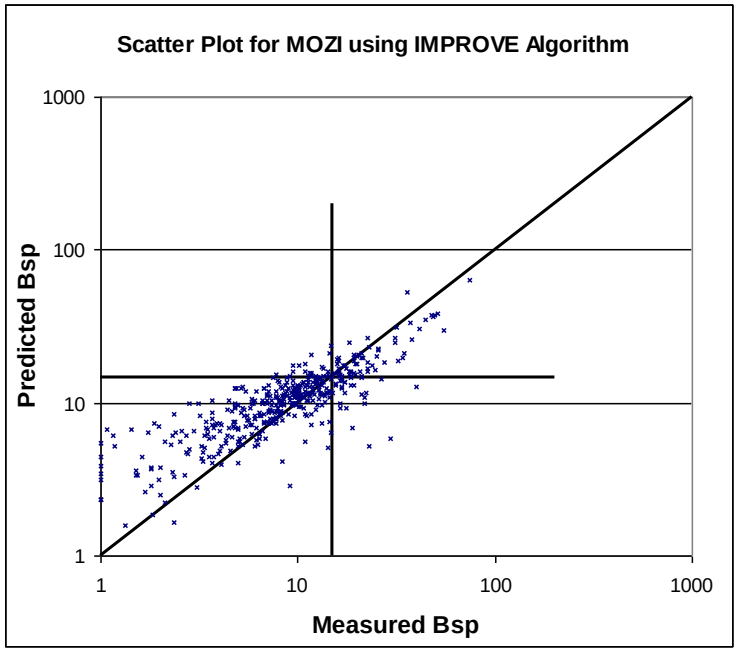
Scatter Plot for MOZI using IMPROVE Algorithm
Predicted Bsp
Measured Bsp
1000
100
10
1
1
10
100
1000

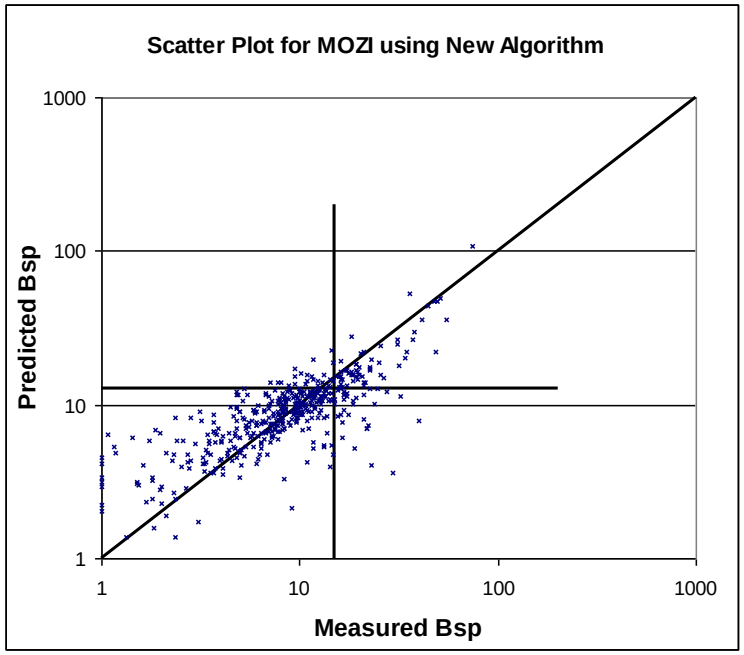
Scatter Plot for MOZI using New Algorithm
Predicted Bsp
Measured Bsp
1000
100
10
1
1
10
100
1000

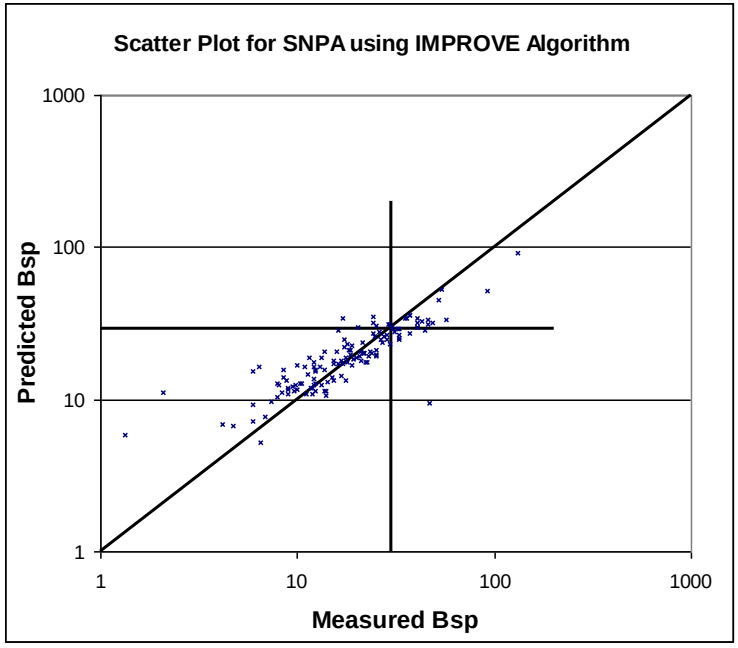
Scatter Plot for SNPA using IMPROVE Algorithm
Predicted Bsp
Measured Bsp
1000
100
10
1
1
10
100
1000

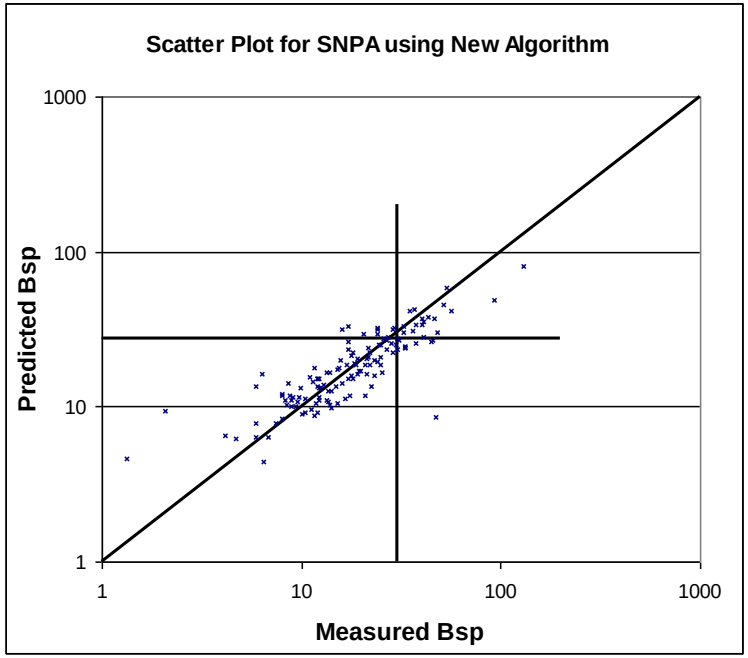
Scatter Plot for SNPA using New Algorithm
Predicted Bsp
Measured Bsp
1000
100
10
1
1
10
100
1000

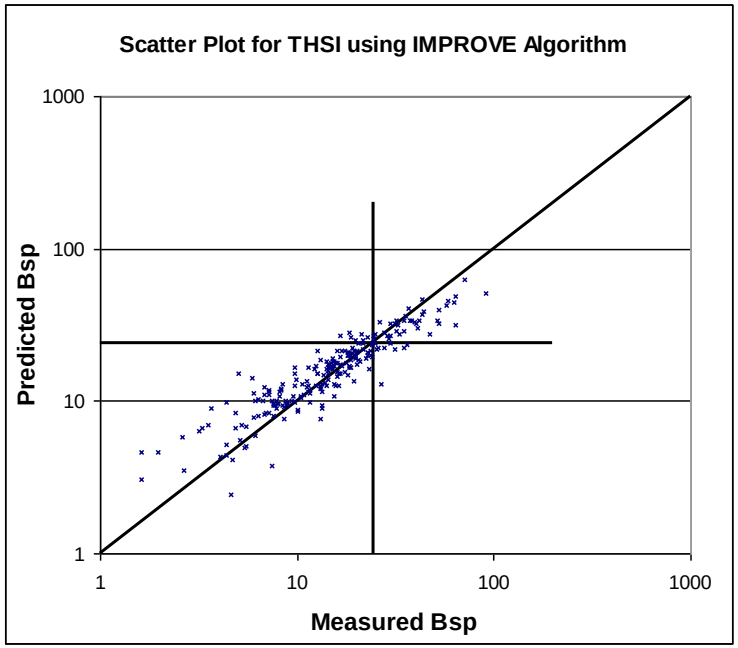
Scatter Plot for THSI using IMPROVE Algorithm
Predicted Bsp
Measured Bsp
1000
100
10
1
1
10
100
1000

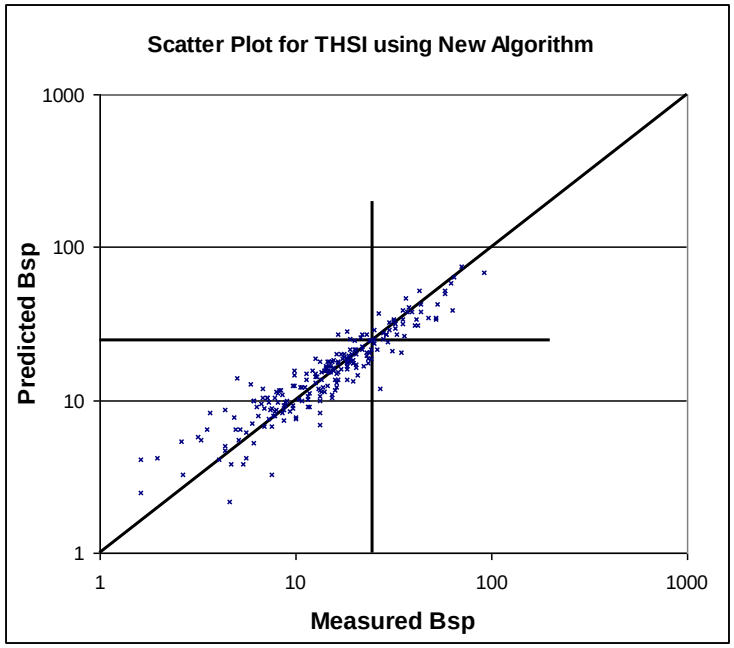
Scatter Plot for THSI using New Algorithm
Predicted Bsp
Measured Bsp
1000
100
10
1
1
10
100
1000

Table A3. Mean light scattering and percent $PM_{2.5}$ composition for the five major components for 20% best days as determined by measurement, the current IMPROVE algorithm and the proposed new algorithm.

Site		Mean Bsp (Mm-1)	Percent Ammonium Sulfate	Percent Ammonium Nitrate	percent OCM	Percent Soil	Percent Coarse	Percent EC
	Measured	6.3	20	3	21	4	50	3
	IMPROVE	8.6	20	3	21	4	49	3
ACAD1	NEW	7.7	20	3	22	4	49	3
	Measured	6.3	17	2	11	10	59	2
	IMPROVE	8.7	19	2	11	9	57	2
BIBE1	NEW	7.9	18	2	11	9	57	2
	Measured	5.4	26	3	21	5	43	2
	IMPROVE	7.7	24	2	23	5	44	2
BOWA1	NEW	6.6	26	3	20	5	44	2
	Measured	5.7	10	3	17	5	61	3
	IMPROVE	8.8	9	4	18	4	62	3
CORI1	NEW	8.4	10	4	18	5	60	4
	Measured	15	26	5	20	4	42	3
	IMPROVE	20	24	6	20	4	42	3
DOSO1	NEW	19	25	6	19	4	42	3
	Measured	2.9	16	2	19	8	52	3
	IMPROVE	4.9	16	2	20	8	50	3
GICL1	NEW	4.1	17	2	20	8	48	3
	Measured	2.0	14	3	15	9	55	2
	IMPROVE	2.8	18	4	16	11	48	3
GRCA2	NEW	2.5	18	5	15	10	48	3
	Measured	5.4	26	3	23	2	43	2
	IMPROVE	8.0	25	4	21	3	44	3
GRGU1	NEW	6.8	25	4	22	3	44	3
	Measured	15	24	6	23	4	39	4
	IMPROVE	20	24	6	24	4	38	4
GRSM1	NEW	20	25	7	23	3	38	4
	Measured	1.8	11	2	21	8	56	2
	IMPROVE	3.6	12	3	22	7	54	2
JARB1	NEW	3.2	12	3	22	7	54	2
	Measured	5.3	12	6	19	9	50	4
	IMPROVE	8.2	12	6	18	10	50	4
LOPE1	NEW	7.2	13	7	18	10	49	4
	Measured	5.3	24	6	25	4	38	3
	IMPROVE	8.2	24	4	27	4	38	3
LYBR1	NEW	7.0	25	5	26	4	38	3
	Measured	18	27	7	21	4	37	3
	IMPROVE	22	25	9	21	4	36	4
MACA1	NEW	19	26	9	20	4	37	4
	Measured	5.5	14	3	31	4	45	4
	IMPROVE	6.8	14	3	27	4	49	3
MORA1	NEW	6.2	14	3	28	4	48	4
MOZI1	Measured	2.8	12	3	18	8	57	2

	IMPROVE	4.8	13	4	18	8	55	3
	NEW	4.1	13	4	17	7	56	3
	Measured	19	21	3	19	3	50	3
	IMPROVE	23	20	3	19	3	52	3
OKEF1	NEW	21	22	3	20	3	49	3
	Measured	11	27	10	18	4	39	3
	IMPROVE	14	26	10	19	4	38	3
SHEN1	NEW	13	26	10	19	4	38	3
	Measured	4.6	16	2	21	6	53	3
	IMPROVE	8.9	19	2	22	4	50	3
SHRO1	NEW	8.0	19	2	21	4	51	3
	Measured	7.3	14	5	22	5	49	4
	IMPROVE	10.0	13	6	26	5	44	5
SNPA1	NEW	8.7	15	7	25	5	43	5
	Measured	5.4	10	2	23	4	58	3
	IMPROVE	7.1	12	3	23	5	54	3
THSI1	NEW	6.4	11	3	22	4	57	3
	Measured	13	15	4	16	5	57	2
	IMPROVE	14	15	6	17	5	55	2
UPBU1	NEW	13	15	6	17	5	55	2

Table A4. Mean light scattering and percent $PM_{2.5}$ composition for the five major components for 20% worst days as determined by measurement, the current IMPROVE algorithm and the proposed new algorithm.

Site		Mean Bsp (Mm-1)	Percent Ammonium Sulfate	Percent Ammonium Nitrate	percent OCM	Percent Soil	Percent Coarse	Percent EC
	Measured	58	34	6	22	3	32	3
	IMPROVE	59	34	6	21	3	33	3
ACAD1	NEW	62	34	6	22	3	33	3
	Measured	49	34	2	16	7	39	2
	IMPROVE	44	33	2	15	8	41	2
BIBE1	NEW	46	33	2	15	8	41	2
	Measured	53	25	13	23	4	32	2
	IMPROVE	49	27	13	22	4	32	2
BOWA1	NEW	45	23	13	23	4	35	2
	Measured	56	13	11	25	5	43	3
	IMPROVE	48	13	10	24	5	45	3
CORI1	NEW	48	12	10	24	5	46	3
	Measured	109	44	2	21	3	28	2
	IMPROVE	105	47	2	21	3	26	2
DOSO1	NEW	121	46	1	20	3	29	2
	Measured	25	18	2	25	8	44	2
	IMPROVE	24	19	2	26	8	43	2
GICL1	NEW	23	18	2	26	9	44	2
	Measured	19	16	3	19	11	50	2
	IMPROVE	19	11	2	18	10	57	1
GRCA2	NEW	18	11	2	18	10	57	1
GRGU1	Measured	58	35	3	24	3	33	3

	IMPROVE	56	36	4	25	3	30	3
	NEW	59	35	3	26	3	30	3
	Measured	153	52	1	22	3	20	2
	IMPROVE	125	51	1	22	3	21	2
GRSM1	NEW	163	52	1	22	3	21	2
	Measured	24	8	3	21	12	54	2
	IMPROVE	21	7	3	20	12	57	1
JARB1	NEW	21	7	3	21	12	57	1
	Measured	35	13	14	20	9	41	3
	IMPROVE	33	12	15	20	9	41	3
LOPE1	NEW	31	11	13	21	9	42	3
	Measured	83	42	8	23	4	21	3
	IMPROVE	75	44	7	21	4	21	3
LYBR1	NEW	77	45	6	22	4	21	3
	Measured	106	42	11	23	3	19	3
	IMPROVE	96	42	9	22	3	21	3
MACA1	NEW	102	42	7	24	3	21	3
	Measured	42	20	3	37	5	31	4
	IMPROVE	42	23	4	35	5	30	4
MORA1	NEW	42	20	3	37	5	32	4
	Measured	24	15	4	23	8	47	2
	IMPROVE	21	15	4	22	8	49	2
MOZI1	NEW	20	13	3	24	9	49	2
	Measured	87	31	3	17	4	43	2
	IMPROVE	75	29	3	18	6	42	2
OKEF1	NEW	76	31	3	17	5	42	2
	Measured	95	46	4	20	4	23	3
	IMPROVE	94	48	5	20	3	22	2
SHEN1	NEW	108	47	3	21	3	24	2
	Measured	77	36	5	20	7	29	3
	IMPROVE	63	35	3	18	7	35	3
SHRO1	NEW	62	36	3	20	6	32	3
	Measured	46	17	7	39	5	26	5
	IMPROVE	36	17	7	35	6	31	5
SNPA1	NEW	37	15	6	37	6	32	5
	Measured	40	12	3	40	5	38	3
	IMPROVE	34	12	3	36	5	41	3
THSI1	NEW	37	12	2	38	5	40	3
	Measured	123	42	3	20	5	27	2
	IMPROVE	104	41	3	20	6	29	2
UPBU1	NEW	124	43	2	21	5	28	2